hep-ph/0101192
CERN-TH/2000-377
GeF/TH/8-00
RM3-TH/00-20

# Polarized Parton Distributions from Charged–Current Deep-Inelastic Scattering and Future Neutrino Factories

Stefano Forte[†]

*INFN, Sezione di Roma III*
*Via della Vasca Navale 84, I-00146 Rome, Italy*

Michelangelo L. Mangano and Giovanni Ridolfi[*]

*Theory Division, CERN*
*CH-1211 Geneva 23, Switzerland*

**Abstract**

We discuss the determination of polarized parton distributions from charged–current deep–inelastic scattering experiments. We summarize the next-to-leading order treatment of charged–current polarized structure functions, their relation to polarized parton distributions and scale dependence, and discuss their description by means of a next-to-leading order evolution code. We discuss current theoretical expectations and positivity constraints on the unmeasured C–odd combinations $\Delta q - \Delta\bar{q}$ of polarized quark distributions, and their determination in charged–current deep–inelastic scattering experiments. We give estimates of the expected errors on charged–current structure functions at a future neutrino factory, and perform a study of the accuracy in the determination of polarized parton distributions that would be possible at such a facility. We show that these measurements have the potential to distinguish between different theoretical scenarios for the proton spin structure.

CERN-TH/2000-377
January 2001

---

[†] On leave from INFN, Sezione di Torino, Italy

[*] On leave from INFN, Sezione di Genova, Italy

## 1. Introduction

Polarized deep-inelastic scattering (DIS) has attracted considerable theoretical [1] and experimental [2] interest since the EMC experimental results in 1988 [3] showed that the proton spin structure is subtler than naive parton expectations might suggest. A first generation of experiments with electron and muon beams, and proton, deuterium and neutron (*i.e.* $^3$He) targets has provided us with information on individual polarized parton distributions which give important clues on the relevant underlying theoretical issues. Several crucial pieces of information, however, are still missing. Specifically, current inclusive DIS experiments only measure the C–even combination $\Delta q + \Delta\bar{q}$ of quark distributions. Moreover, they are only very weakly sensitive to the size of the strange quark distribution. Therefore, a full flavor separation is very difficult, and a separate measurement of the quark and antiquark components is impossible. Furthermore, there are indications [4,5] that the polarized gluon distribution is large, but uncertainties are still sizable. Several of these pieces of information are crucial not only in reconstructing the full spin structure of the nucleon, but also (perhaps more interestingly) in deciding among the various theoretical scenarios which have been proposed to understand the somewhat puzzling picture which the original EMC results and their subsequent refinements point at. In particular, it is crucial to determine accurately the size of the strange contribution [6] and of the polarized gluon [7].

In the unpolarized case, the most precise available information on the strange quark distribution and the quark–antiquark separation comes from charged–current deep-inelastic scattering [8], which, being mediated by a charged current, gives access to the flavor structure of the target. In the polarized case, the luminosity of existing neutrino beams requires targets whose typical sizes are of the orders of several meters, and therefore cannot be polarized. In principle, charged–current events can be a significant part of the cross section even with electron or muon beams if the energy is high enough. Indeed, charged–current unpolarized cross sections and structure functions have been measured at HERA [9], and the corresponding polarized asymmetries have been studied [10] as a way of gaining information on polarized parton distributions if the polarized option were to be available at HERA.

It is several years now since muon storage rings have been proposed as a powerful new way to reach high energies and luminosities in a colliding-beam facility [11,12]. It has since been recognized that exciting physics can also be obtained with the highly focused neutrino beams arising from the decays of muons along straight sections of the accumulator [13]. In addition to the obvious applications for studies of neutrino properties (masses and mixings) using far-away detectors (for a recent detailed study see Ref. [14]), DIS experiments operating close-by downstream the muon ring could provide significant contributions to several topics [15,16]: from the study of the nucleon structure to accurate measurement of the parameters of weak and strong interactions, from the determination of CKM matrix elements to studies of heavy quark decays, and more. Reference [15] pointed out the potential for measurements of unparalleled precision of both unpolarized and polarized neutrino structure functions, leading to an accurate decomposition of the partonic content of the nucleon in terms of individual (possibly spin-dependent) flavor densities. A more quantitative investigation of polarized DIS with neutrino beams is therefore called

for, both in order to assess the physics potential of these experiments, and also to decide among other possible options, such as polarized HERA. A first study in this direction has recently appeared in [17].

Several studies of polarized neutrino DIS have been presented in the literature. In particular, the parton model formalism has been presented in Ref. [18], while its relation to perturbative QCD has been worked out through the operator–product expansion at leading order in Refs. [19,20]. The next-to-leading order coefficient functions were computed several years ago [21], and have been recently generalized to the case where heavy quark masses are retained [22]; next-to-leading order polarized anomalous dimensions were determined for the full set of operators relevant to both neutral– and charged–current DIS recently [23]. Even though all the theoretical tools which are needed in order to perform a full next-to-leading order analysis are thus essentially available in the literature, no such study has been performed yet.

In this paper, we wish to give a first systematic next-to-leading order treatment of charged–current polarized DIS. The purpose of this work is to provide a set of common theoretical tools, as well as some benchmark estimates for future work. We will start (Sect. 2) by recalling the structure of the polarized asymmetries in charged–current DIS in terms of structure functions, review their leading–order expressions in terms of parton distributions, and the scale dependence of the parton distributions. We will then recall how charged–current lepton and antilepton DIS on proton and neutron targets allows a full flavor decomposition of the nucleon spin content. In Sect. 3, we will discuss the full next-to-leading order formalism for structure functions and parton distributions (this section can be skipped by those who are only interested in the phenomenological analysis). The results presented here have been incorporated in an upgrade of the ABFR [4] next-to-leading order evolution code for polarized parton distributions, by including the option of evolving charged–current structure functions and fitting them to experimental data. We will next (Sect. 4) discuss the constraints that the elementary requirement of positivity of cross–sections imposes on the otherwise unknown C–odd combinations of quark and antiquark distributions $\Delta q_i - \Delta \bar{q}_i$, and how they limit the set of possible expected results for these quantities. Then, we will examine the current theoretical expectations for the strange and quark-antiquark content of the nucleon within several theoretical scenarios which have been suggested in order to understand current information on the nucleon spin.

We will turn to phenomenology in Sect 5, where we will discuss the precision on the determination of structure functions which is expected at a future muon storage ring facility: in particular, we will review the expected characteristics of the neutrino beam, and present detailed estimates of the expected percentage error on structure function determinations as a function of the kinematic variables $x$ and $Q^2$. We will then (Sect. 6) study how such a determination of polarized structure functions would improve our knowledge of parton distributions: we will generate pseudo–data according to the theoretical scenarios of Sect. 4, distributed according to to the error estimates of Sect. 5, and use the evolution code discussed in Sect. 3 to perform next-to-leading order fits of structure functions to these data. We will thus be able to assess the error on individual parton distributions which would be obtained thanks to this kind of experiment.

## 2. Flavor content and scale dependence of polarized structure functions

Polarized structure functions for charged–current DIS have been computed in the parton model in Ref. [18], and at leading order in perturbative QCD with operator methods in Refs. [19,20]. Here for completeness we briefly review the derivation of the leading order expression of these structure functions from the QCD improved parton model, the evolution equations which govern their scale dependence, and then review how it is possible to use this information to disentangle the polarized flavor and antiflavor content of the target.

### *2.1. Structure functions and parton distributions*

We define structure functions in terms of the hadronic tensor $W^{\mu\nu}$ as follows:

$$\begin{aligned} W_{\mu\nu} = & \left(-g_{\mu\nu} + \frac{q_\mu q_\nu}{q^2}\right) F_1(x,Q^2) + \frac{\hat{p}_\mu \hat{p}_\nu}{p\cdot q} F_2(x,Q^2) + i\epsilon_{\mu\nu\alpha\beta}\frac{q^\alpha p^\beta}{2p\cdot q} F_3(x,Q^2) \\ & - i\epsilon_{\mu\nu\alpha\beta}\frac{q^\alpha s^\beta}{p\cdot q} g_1(x,Q^2) - i\epsilon_{\mu\nu\alpha\beta}\frac{q^\alpha \left(p\cdot q\, s^\beta - s\cdot q\, p^\beta\right)}{(p\cdot q)^2} g_2(x,Q^2) \\ & + \frac{1}{p\cdot q}\left[\frac{1}{2}\left(\hat{p}_\mu \hat{s}_\nu + \hat{p}_\nu \hat{s}_\mu\right) - \frac{s\cdot q}{p\cdot q}\hat{p}_\mu \hat{p}_\nu\right] g_3(x,Q^2) \\ & + \frac{s\cdot q}{p\cdot q}\left[\frac{\hat{p}_\mu \hat{p}_\nu}{p\cdot q} g_4(x,Q^2) + \left(-g_{\mu\nu} + \frac{q_\mu q_\nu}{q^2}\right) g_5(x,Q^2)\right], \end{aligned} \tag{2.1}$$

where $q^\mu$, $p^\mu$ and $s^\mu$ are respectively the momentum of the incoming virtual gauge bosons, and the momentum and spin of the incoming nucleon, and

$$\hat{p}_\mu \equiv p_\mu - \frac{p\cdot q}{q^2} q_\mu; \qquad \hat{s}_\mu \equiv s_\mu - \frac{s\cdot q}{q^2} q_\mu. \tag{2.2}$$

The proton spin vector is normalized as $s^2 = -m^2$, where $m$ is the hadron mass. The hadronic tensor is defined as [24]

$$W_{\mu\nu} = \frac{1}{4\pi}\int d^4z\, e^{iq\cdot z}\, \langle p,s|\left[J_\mu(z), J_\nu^\dagger(0)\right]|p,s\rangle. \tag{2.3}$$

Notice that the definition with $\mu \leftrightarrow \nu$ is sometimes (*e.g.* in [18]) adopted; this corresponds to changing the sign of the antisymmetric part of the tensor. The definitions of the unpolarized structure functions $F_i$ and of the polarized parity-conserving structure functions $g_1$, $g_2$ are essentially standard, while a variety of different conventions have been adopted in the literature for the polarized parity-violating structure functions $g_3$, $g_4$ and $g_5$. Here we adopt the same convention as Ref. [20].

We now specialize to the case of charged–current scattering. The total cross section for charged–current DIS on unpolarized targets is given by

$$\frac{d^2\sigma^{\lambda_\ell}(x,y,Q^2)}{dxdy} = \frac{G_F^2}{2\pi(1+Q^2/m_W^2)^2}\frac{Q^2}{xy}\left[-\lambda_\ell\, y\left(1-\tfrac{y}{2}\right) xF_3 + (1-y-x^2y^2\tfrac{m^2}{Q^2})F_2 + y^2 xF_1\right] \tag{2.4}$$

where $\lambda_\ell = \pm 1$ is the helicity of the incoming lepton ($-1$ for a neutrino or electron, $+1$ for an antineutrino or positron). The explicit expressions of the various structure functions in eq. (2.4) depend only on the charge of the exchanged $W$, and on the target. The polarized cross-section difference

$$\Delta\sigma \equiv \sigma(\lambda_p = -1) - \sigma(\lambda_p = +1), \tag{2.5}$$

where $\lambda_p = \pm 1$ is the proton helicity, is given by

$$\begin{aligned}\frac{d^2\Delta\sigma^{\lambda_\ell}(x,y,Q^2)}{dxdy} =& \frac{G_F^2}{\pi(1+Q^2/m_W^2)^2}\frac{Q^2}{xy}\Bigg\{ \left[-\lambda_\ell\, y(2-y)xg_1 - (1-y)g_4 - y^2 x g_5\right] \\ &+ 2xy\frac{m^2}{Q^2}\left[\lambda_\ell x^2y^2 g_1 + \lambda_\ell 2x^2 y g_2 + \left(1 - y - x^2y^2\tfrac{m^2}{Q^2}\right)xg_3\right. \\ &\left. -x\left(1 - \tfrac{3}{2}y - x^2y^2\tfrac{m^2}{Q^2}\right)g_4 - x^2y^2 g_5\right]\Bigg\}. \end{aligned} \tag{2.6}$$

The results in eqs. (2.4) and (2.6) agree with those given in Ref. [18], while they are by a factor of two larger than the results of Ref. [20]. The definition eq. (2.5) corresponds to the difference of antiparallel minus parallel spins of the incoming particles for an incoming lepton, but parallel minus antiparallel spins for an incoming antilepton.

Equation (2.6) shows that for longitudinal nucleon polarization the contributions of the structure functions $g_2$ and $g_3$ to the cross–section are suppressed by powers of $\frac{m^2}{Q^2}$. These structure functions give an unsuppressed contribution to the cross–section for transverse polarization, but in such case the polarized cross section difference itself vanishes as $\frac{m^2}{Q^2} \to 0$. Henceforth, we will systematically neglect all power suppressed contributions; therefore, we will not discuss these structure functions further. It should be pointed out, however, that at the neutrino factory it will be possible in principle to extract the power-suppressed contributions directly from the data, by studying the $Q^2$ dependence.

Because the same tensor structures appear in the spin-dependent and spin-independent parts of the hadronic tensor eq. (2.1) in the $\frac{m^2}{Q^2} \to 0$ limit, the cross section difference eq. (2.6) is obtained from the total cross-section eq. (2.4) replacing

$$F_1 \to -g_5, \quad F_2 \to -g_4, \quad F_3 \to 2g_1 \tag{2.7}$$

and multiplying by a factor two due to the fact that the total cross–section is an average over initial state polarizations. In particular, it is easy to derive a polarized analogue [25] of the Callan-Gross relation [26], which follows from the observation that the quark-gluon coupling conserves helicity when all masses are neglected, so the hadronic tensor eq. (2.1), if computed at leading order, must vanish when contracted with a longitudinal polarization vector $\epsilon_\nu^L$. Since $\epsilon_\nu^L$ can be written as a linear combination of $p$ and $q$, this condition implies $p_\mu p_\nu W^{\mu\nu} = 0$, which using the expression eq. (2.1) becomes

$$p_\mu p_\nu W^{\mu\nu} = \frac{(p\cdot q)^2}{q^2}\left[\left(F_1 - \frac{F_2}{2x}\right) + \frac{s\cdot q}{p\cdot q}\left(g_5 - \frac{g_4}{2x}\right)\right] = 0. \tag{2.8}$$

Therefore at leading order

$$g_4(x,Q^2) = 2x g_5(x,Q^2), \tag{2.9}$$

and, at leading twist, there are only two independent polarized structure functions, namely $g_1$ (parity conserving) and $g_5$ (parity violating), respectively analogous to the unpolarized structure functions $F_1$ and $F_3$. We will see in Sect. 3.1 that also beyond leading order there are only two independent structure functions, despite the fact that eq. (2.9) is violated.

The leading–order expression of $g_1$ and $g_5$ are straightforwardly found by computing the hadronic tensor for $W^\pm$ scattering off a free quark [18]:

$$\begin{aligned}
g_1^{W^+}(x,Q^2) &= \Delta\bar{u}(x,Q^2) + \Delta d(x,Q^2) + \Delta\bar{c}(x,Q^2) + \Delta s(x,Q^2) \\
g_1^{W^-}(x,Q^2) &= \Delta u(x,Q^2) + \Delta\bar{d}(x,Q^2) + \Delta c(x,Q^2) + \Delta\bar{s}(x,Q^2) \\
g_5^{W^+}(x,Q^2) &= \Delta\bar{u}(x,Q^2) - \Delta d(x,Q^2) + \Delta\bar{c}(x,Q^2) - \Delta s(x,Q^2) \\
g_5^{W^-}(x,Q^2) &= -\Delta u(x,Q^2) + \Delta\bar{d}(x,Q^2) - \Delta c(x,Q^2) + \Delta\bar{s}(x,Q^2).
\end{aligned} \tag{2.10}$$

Below charm threshold only the Cabibbo-suppressed part of the $\Delta s$ contribution survives, because the Cabibbo-enhanced transition would require production of a $c$ quark in the final state. A $\Delta c$ contribution is in principle possible even below charm threshold in case intrinsic charm [27] is present, since it only requires production of a strange quark. Similarly, the Cabibbo-suppressed part of the down contribution vanishes. Hence, below charm threshold the leading–order expression of the structure functions is

$$\begin{aligned}
g_1^{W^+}(x,Q^2) &= \Delta\bar{u}(x,Q^2) + \cos^2\theta_c \Delta d(x,Q^2) + \Delta\bar{c}(x,Q^2) + \sin^2\theta_c \Delta s(x,Q^2) \\
g_1^{W^-}(x,Q^2) &= \Delta u(x,Q^2) + \cos^2\theta_c \Delta\bar{d}(x,Q^2) + \Delta c(x,Q^2) + \sin^2\theta_c \Delta\bar{s}(x,Q^2) \\
g_5^{W^+}(x,Q^2) &= \Delta\bar{u}(x,Q^2) - \cos^2\theta_c \Delta d(x,Q^2) + \Delta\bar{c}(x,Q^2) - \sin^2\theta_c \Delta s(x,Q^2) \\
g_5^{W^-}(x,Q^2) &= -\Delta u(x,Q^2) + \cos^2\theta_c \Delta\bar{d}(x,Q^2) - \Delta c(x,Q^2) + \sin^2\theta_c \Delta\bar{s}(x,Q^2),
\end{aligned} \tag{2.11}$$

where $\theta_c$ is the Cabibbo angle, and $\Delta c$ is the intrinsic charm distribution. The remaining mixing angles in the CKM matrix can be taken to vanish for all practical purposes, so a contribution from $\Delta b$ will only be present above the top threshold; it will then have the form which straightforwardly follows from repeating the pattern of previous generations. Equation (2.10) is to be contrasted with the familiar case of virtual photon scattering, where

$$\begin{aligned}
g_1^{\gamma^*}(x,Q^2) &= \frac{1}{2}\sum_{i=1}^{n_f} e_i^2 \left[\Delta q_i(x,Q^2) + \Delta\bar{q}_i(x,Q^2)\right] \\
g_5^{\gamma^*}(x,Q^2) &= 0.
\end{aligned} \tag{2.12}$$

*2.2. Evolution equations*

The scale dependence of parton distributions is determined by the Altarelli-Parisi evolution equations [28,29]. Define the C–even and C–odd quark distributions

$$\Delta q_i^\pm = \Delta q_i \pm \Delta q_i, \tag{2.13}$$

the singlet combination

$$\Delta\Sigma^{\pm} = \sum_{i=1}^{n_f} \Delta q_i^{\pm}; \qquad \Delta\Sigma \equiv \Delta\Sigma^{+} \tag{2.14}$$

and the nonsinglet combination

$$\Delta q_{ij}^{NS\,\pm} = \left(\Delta q_i^{\pm} - \Delta q_j^{\pm}\right), \quad i \neq j. \tag{2.15}$$

The evolution equations have the form

$$\begin{aligned}
&\frac{d}{dt}\Delta q_{ij}^{NS\,\pm} = \frac{\alpha_s(t)}{2\pi}\Delta P_{NS}^{\pm} \otimes \Delta q_{ij}^{NS\,\pm}, \\
&\frac{d}{dt}\Delta\Sigma^{-} = \frac{\alpha_s(t)}{2\pi}\Delta P_{S}^{-} \otimes \Delta\Sigma^{-}, \\
&\frac{d}{dt}\begin{pmatrix}\Delta\Sigma \\ \Delta g\end{pmatrix} = \frac{\alpha_s(t)}{2\pi}\begin{pmatrix}\Delta P_S^{+} & 2n_f\Delta P_{qg} \\ \Delta P_{gq} & \Delta P_{gg}\end{pmatrix} \otimes \begin{pmatrix}\Delta\Sigma \\ \Delta g\end{pmatrix},
\end{aligned} \tag{2.16}$$

where $t = \log\left(Q^2/\Lambda^2\right)$, $\otimes$ denotes the usual convolution with respect to $x$, and all splitting functions admit a perturbative expansion of the form $\Delta P(x,\alpha_s) = \Delta P^{(0)} + \frac{\alpha_s}{2\pi}\Delta P^{(1)} + \ldots$.

Notice that the gluon distribution cannot mix with the C–odd distributions because charge conjugation implies that

$$P_{qg} = P_{\bar{q}g}; \qquad P_{gq} = P_{g\bar{q}}. \tag{2.17}$$

Furthermore, because all flavors are equivalent when masses are neglected, it is only necessary to distinguish flavor-conserving (diagonal) splittings $P_{qq}^{D} \equiv P_{q_iq_i}$ and flavor-changing (non-diagonal) splittings $P_{qq}^{ND} \equiv P_{q_iq_j}$ with $i \neq j$. Finally, also by charge conjugation,

$$P_{q\bar{q}} = P_{\bar{q}q}, \quad P_{\bar{q}\bar{q}} = P_{qq}; \qquad \Delta P_{q\bar{q}} = \Delta P_{\bar{q}q}; \quad \Delta P_{\bar{q}\bar{q}} = \Delta P_{qq}. \tag{2.18}$$

It then follows immediately that, in general

$$\begin{aligned}
\Delta P_{NS}^{\pm} &= \left(\Delta P_{qq}^{D} - \Delta P_{qq}^{ND}\right) \pm \left(\Delta P_{q\bar{q}}^{D} - \Delta P_{q\bar{q}}^{ND}\right) \\
\Delta P_{S}^{\pm} &= \left(\Delta P_{qq}^{D} + (n_f-1)\Delta P_{qq}^{ND}\right) \pm \left(\Delta P_{q\bar{q}}^{D} + (n_f-1)\Delta P_{q\bar{q}}^{ND}\right),
\end{aligned} \tag{2.19}$$

similarly to the unpolarized case (with $P \to \Delta P$).

Specializing now to the leading–order case, note that, because the quark–gluon interaction conserves helicity, flavor, and baryon number, at leading order there is only one quark-quark splitting function

$$P_{q_iq_i}^{\mathrm{LO}} = \Delta P_{q_iq_i}^{\mathrm{LO}} \equiv P_{qq}^{\mathrm{LO}}, \tag{2.20}$$

while

$$\begin{aligned}
P_{q\bar{q}}^{\mathrm{LO}} &= \Delta P_{q\bar{q}}^{\mathrm{LO}} = 0 \\
P_{qq}^{ND,\,\mathrm{LO}} &= \Delta P_{qq}^{ND,\,\mathrm{LO}} = 0.
\end{aligned} \tag{2.21}$$

It follows that at leading order all quark (polarized and unpolarized) distributions evolve with the same splitting function:

$$\Delta P^- \equiv \Delta P_{NS}^{-,\,\mathrm{LO}} = \Delta P_{NS}^{+,\,\mathrm{LO}} = \Delta P_{S}^{\pm,\,\mathrm{LO}} = P_{qq}^{\mathrm{LO}}. \tag{2.22}$$

*2.3. Flavor decomposition*

Assuming the availability of neutrino and antineutrino beams, and the capability of measuring independently $g_1$ and $g_5$, we have four different linear combinations of individual polarized parton distributions from charged–current scattering, on top of the usual one (or two, if proton and neutron targets are available) from neutral–current scattering. Using the leading order expressions of the structure functions, eq. (2.10), we get

$$\tfrac{1}{2}\left(g_1^{W^-} - g_5^{W^-}\right) = \Delta u + \Delta c; \qquad \tfrac{1}{2}\left(g_1^{W^+} + g_5^{W^+}\right) = \Delta \bar{u} + \Delta \bar{c}; \tag{2.23}$$

$$\tfrac{1}{2}\left(g_1^{W^+} - g_5^{W^+}\right) = \Delta d + \Delta s; \qquad \tfrac{1}{2}\left(g_1^{W^-} + g_5^{W^-}\right) = \Delta \bar{d} + \Delta \bar{s}. \tag{2.24}$$

Below charm threshold, in the absence of intrinsic charm, and neglecting Cabibbo-suppressed contributions, the $\Delta c$ and $\Delta s$ contributions decouple, and all four light flavors and antiflavors can be extracted directly from eqs. (2.23),(2.24). Above charm threshold, or even below threshold if intrinsic charm is present, a direct measurement of all individual parton distributions is only possible if further independent linear combinations are experimentally available.

For a nucleon target, further independent linear combinations of parton distributions can be determined by using both proton and neutron (or deuterium) targets: by isospin, all structure functions for a neutron target are expressed in terms of parton distributions of the proton by interchanging $u$ and $d$ in the expressions for a proton target. This then gives us four new combinations, obtained interchanging $u$ and $d$ in eqs. (2.23),(2.24). Combining these with the combinations eqs. (2.23),(2.24), however, only gives us six independent linear combinations. A convenient choice is for instance

$$\tfrac{1}{2}\left(g_1^{W^+} - g_5^{W^+}\right)[n-p] = \Delta u - \Delta d; \quad \tfrac{1}{2}\left(g_1^{W^-} + g_5^{W^-}\right)[n-p] = \Delta \bar{u} - \Delta \bar{d}; \tag{2.25}$$

$$\tfrac{1}{2}\left(g_1^{W^-} - g_5^{W^-}\right)[p] - \tfrac{1}{2}\left(g_1^{W^+} - g_5^{W^+}\right)[n] = \Delta s - \Delta c;$$

$$\tfrac{1}{2}\left(g_1^{W^-} + g_5^{W^-}\right)[p] - \tfrac{1}{2}\left(g_1^{W^+} + g_5^{W^+}\right)[n] = \Delta \bar{s} - \Delta \bar{c}; \tag{2.26}$$

$$\tfrac{1}{2}\left(g_1^{W^+} - g_5^{W^+}\right)[p+n] = \Delta u + \Delta d + 2\Delta s;$$

$$\tfrac{1}{2}\left(g_1^{W^-} + g_5^{W^-}\right)[p+n] = \Delta \bar{u} + \Delta \bar{d} + 2\Delta \bar{s}. \tag{2.27}$$

The structure functions measured from virtual photon scattering eq. (2.12) do not provide any further independent linear combination of parton distributions.

It follows that a complete separation of the four active flavors and antiflavors at a fixed scale above charm threshold from inclusive nucleon structure functions only is not possible. However, the separation is possible by comparing structure functions above

and below threshold. For instance, neglecting Cabibbo-suppressed terms, below charm threshold eq. (2.24) determines the down polarized (quark and antiquark) distributions, eq. (2.26) gives the (intrinsic) charm, and then either eq. (2.23) or eq. (2.25) give the up distribution, the other equation providing a consistency check. Hence, the up, down and (intrinsic) charm can always be determined below threshold. In fact, the deviation from zero of eq. (2.26) provides a simple way of testing for the presence of intrinsic charm or anticharm, at least within the limitations of the leading–order approximation. The strange distribution can be determined by comparing *e.g.* eq. (2.24) below and above threshold.

Alternatively, above threshold, individual flavor contributions to the structure functions can be separated by tagging the final-state quark: *e.g.* the strange contribution can be measured by tagging charm in the final state, as is routinely done in unpolarized experiments [8]. A simpler option consists in assuming that the charm distribution vanishes below threshold, and is generated dynamically by perturbative evolution above threshold. In such case, as mentioned above, the up and down components can be determined from eqs. (2.23),(2.24) below threshold, and the strange distribution can then be determined from eqs. (2.26),(2.27) above threshold.

As already mentioned, the virtual photon structure functions eq. (2.12) do not provide any further information. However, they do provide independent consistency checks. Specifically, as is well known, the isotriplet combination of $g_1^{\gamma^*}$ is particularly interesting in that its first moment is determined by the Bjorken sum rule. Now, the same isotriplet combination of parton distributions is measured by neutral–current and charged–current structure functions:

$$6g_1^{\gamma^*}[p-n] = \left(g_5^{W^+} - g_5^{W^-}\right)[p-n] = (\Delta u + \Delta\bar{u}) - \left(\Delta d + \Delta\bar{d}\right). \tag{2.28}$$

Likewise, the strange distribution can be also determined by combining neutral– and charged–current structure functions:

$$6g_1^{\gamma^*}[p+n] - \tfrac{5}{3}\left(g_1^{W^+} + g_1^{W^-}\right)[p] = \left(g_5^{W^+} - g_5^{W^-}\right)[p+n] = (\Delta c + \Delta\bar{c}) - (\Delta s + \Delta\bar{s}). \tag{2.29}$$

Finally, notice that a determination of the pure singlet quark distribution $\Delta\Sigma$ eq.(2.14) can be directly obtained combining charged–current $g_1$ data:

$$\left(g_1^{W^+} + g_1^{W^-}\right)[p] = \left(g_1^{W^+} + g_1^{W^-}\right)[n] = \Delta\Sigma^+. \tag{2.30}$$

This is to be contrasted with the analogous measurement obtained from global fits to $g_1^{\gamma^*}$ data, which can only be done (for first moments) using information from octet $\beta$–decays and SU(3) symmetry, or else (for all moments) by using scaling violations. A potentially very accurate measurement of this quantity, whose smallness is at the origin of the so-called 'nucleon spin crisis', is thus possible.

Of course, all combinations of parton distributions given in this section are only correct at leading order, and may thus only be used for rough estimates. Next-to-leading order corrections, which are necessary for a more detailed treatment, would modify these relations. In practice, an accurate determination of parton distributions can be achieved by means of a global fit, which will include all these relations and their next-to-leading order modifications.

## 3. Structure functions and parton distributions at next-to-leading order

Beyond leading order, structure functions are no longer linear combinations of quark distributions, rather, they are obtained by convoluting quark and gluon distributions with perturbative coefficient functions; furthermore, the splitting functions which govern their evolution eq. (2.16) acquire a dependence on $Q^2$ through $\alpha_s$, and in particular no longer satisfy the simple relations eqs. (2.20)-(2.21).

### *3.1. Next-to-leading coefficient functions*

The general expression of the leading–twist polarized charged–current structure functions beyond leading order is

$$\begin{aligned} g_1^{W^\pm}(x,Q^2) &= \frac{1}{2}\left[\Delta C_{\Sigma^+}\otimes\Delta\Sigma^+ \mp \Delta C_{NS\,-}\otimes\left(\Delta q_{ud}^{NS\,-}+\Delta q_{cs}^{NS\,-}\right)\right] + 2[n_f/2]\Delta C_g\otimes\Delta g \\ g_i^{W^\pm}(x,Q^2) &= -\frac{1}{2}\left[\Delta C^i_{\Sigma^-}\otimes\Delta\Sigma^- \mp \Delta C^i_{NS\,+}\otimes\left(\Delta q_{ud}^{NS\,+}+\Delta q_{cs}^{NS\,+}\right)\right],\ i=4,5, \end{aligned} \tag{3.1}$$

where $n_f$ is the number of active flavors, and $[n_f/2]$ is the integer part of $n_f/2$. In this equation, $\Delta g$ is the polarized gluon distribution, the singlet quark distribution $\Delta\Sigma^\pm$ and nonsinglet distributions $\Delta q_{ij}^{NS\,\pm}$ were defined in eq. (2.14) and eq. (2.15) respectively, and all coefficient functions admit a perturbative expansion of the form $\Delta C(x,\alpha_s) = \Delta C^{(0)} + \frac{\alpha_s}{2\pi}C^{(1)}(x,\alpha_s)+\ldots$, where $\Delta C^{(0)} = \delta(1-x)$ for all the quark coefficient functions in eq. (3.1), and $\Delta C_g^{(0)} = 0$ for the gluon coefficient function. Notice that the polarized gluon distribution contributes to the structure function $g_1$, but decouples from $g_4$ and $g_5$ by charge conjugation.

To next-to-leading order, in fact, for each of the three structure functions all quark coefficient functions are equal in standard factorization schemes such as $\overline{\rm MS}$:

$$\begin{aligned} \Delta C_{\Sigma^+}{}^{(1)}(x) &= \Delta C_{NS\,-}{}^{(1)}(x) \equiv \Delta C_q{}^{(1)}(x) \\ \Delta C^i_{\Sigma^-}{}^{(1)}(x) &= \Delta C^i_{NS\,+}{}^{(1)}(x) \equiv \Delta C_i{}^{(1)}(x), \quad i=4,5 \end{aligned} \tag{3.2}$$

so that eq. (3.1) reduces to the simpler expression

$$\begin{aligned} g_1^{W^\pm;\,\rm NLO}(x,Q^2) &= \Delta C_q\otimes g_1^{W^\pm,\,\rm LO} + 2[n_f/2]\,\Delta C_g\otimes\Delta g \\ g_i^{W^\pm,\,\rm NLO}(x,Q^2) &= \Delta C_i\otimes g_i^{W^\pm,\,\rm LO}, \quad i=4,5, \end{aligned} \tag{3.3}$$

where $g^{W^\pm;\,\rm LO}$ are the leading–order expressions of the various structure functions, given by eq. (2.10) above charm threshold and eq. (2.11) below charm threshold. Note, however, that the simple relations eqs. (3.2) are already violated at order $\alpha_s^2$ in the $\overline{\rm MS}$ scheme [30].

The next-to-leading coefficient functions for virtual photon DIS structure functions have been known for some time [31]. Because the underlying partonic subprocesses are the same, the $g_1$ coefficient functions for charged–current and neutral–current scattering in fact coincide: the only difference is in the couplings between gauge bosons and quarks,

which is reflected in the different leading–order expressions eq. (2.10) and eq. (2.12). As is by now well known [1], the first moment of the singlet polarized quark distributions has an O(1) scheme dependence, due to the fact that at leading order the first moment $\Delta g(1)$ of the gluon distribution evolves as $1/\alpha_s$, *i.e.* $\alpha_s \Delta g(1)$ is scale independent up to next-to-leading corrections. This is a consequence [32] of the anomaly which affects the singlet axial current. A further consequence of this is that it is possible to choose the factorization scheme in such a way that the first moment of the singlet quark distribution is scale independent (to all perturbative orders), even though this is not the case in the $\overline{\rm MS}$ scheme. This choice is particularly convenient in that it allows a meaningful comparison with constituent quark model predictions and expectations, which are scale independent. Even after fixing by this requirement the scheme ambiguity on the quark first moment, there remains a residual ambiguity on the other moments, which can be fixed in a minimal way by requiring the scheme-change matrix from the $\overline{\rm MS}$ scheme to be $x$-independent. This defines the so-called Adler-Bardeen (AB) scheme [33].

The first moment of any quark distribution in the $\overline{\rm MS}$ and AB schemes are related by

$$\Delta q_i^{\overline{\rm MS}}(1,Q^2) = \Delta q_i^{\rm AB}(1) - \frac{\alpha_s}{4\pi}\Delta g(1,Q^2), \tag{3.4}$$

where $\Delta q(1,Q^2) = \int_0^1 dx \Delta q(x,Q^2)$. Correspondingly, the first moment $\Delta C_g(1,\alpha_s)$ of the gluon coefficient function vanishes in the $\overline{\rm MS}$ scheme, while in the AB scheme it is equal to $\Delta C_g^{\rm AB}(1,\alpha_s) = -\frac{\alpha_s}{4\pi}$. Notice that, below charm threshold, scheme invariance of the physically observable structure function $g_1^{W^\pm}$ eq. (3.1) upon this scheme change (and more generally upon any scheme change which mixes the quark singlet and gluon distributions) is ensured by the fact that the mixing with the gluon of $\Delta s$ and $\Delta d$ contributions combine to give one effective active flavor. The explicit expressions of the quark and gluon $g_1$ coefficient functions are given *e.g.* in Ref. [33].

The next-to-leading order coefficient functions for the structure functions $g_4$ and $g_5$ have been computed in Ref. [21]. Both in the $\overline{\rm MS}$ and AB schemes, they are simply related to the $g_1$ quark coefficient function by

$$\begin{aligned} \Delta C_4^{(1)}(x) &= \Delta C_q^{(1)}(x) + C_F x(1+x) \\ \Delta C_5^{(1)}(x) &= \Delta C_q^{(1)}(x) + C_F x(1-x), \end{aligned} \tag{3.5}$$

where $C_F = \frac{N_c^2-1}{2N_c}$. The fact that these coefficient functions are unequal to each other implies in particular that the Callan-Gross-like relation, eq. (2.9), is violated beyond leading order, as expected since the helicity conservation on which it was based only holds at leading order. In fact, the relations between the three quark coefficient functions eq. (3.5) are the same as the corresponding relations between unpolarized quark coefficient functions which are obtained by the replacements eq. (2.7), again due to the fact that the corresponding tensor structures in eq. (2.1) are the same. However, by charge conjugation, there is no gluon contribution to either $g_4$ or $g_5$, so the violation of eq. (2.9) is entirely given by eq. (3.5), contrary to the unpolarized case where the Callan-Gross relation is also violated by a gluon contribution. Hence, unlike $F_1$ and $F_2$ which, beyond leading order,

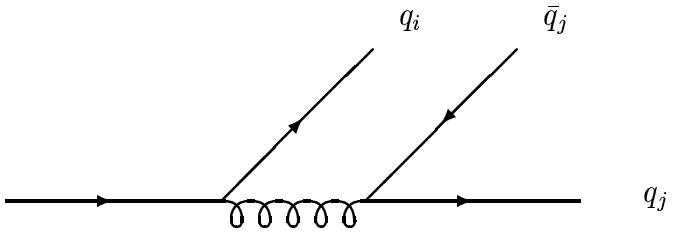


Figure 1: The lowest–order diagram which contributes to $P_{q\bar{q}}$ and $P_{qq}^{ND}$.

measure different combinations of parton distributions (so in particular their comparison allows a direct extraction of the gluon distribution), $g_4$ and $g_5$ measure the same combination of parton distributions, and thus their separate determination does not provide any extra information. Therefore, we will henceforth only discuss the structure function $g_5$, since $g_4$ can be entirely determined from it. Once again, this fact can be tested directly on the data, by performing a three-parameter (*i.e.* $g_1$, $g_4$, and $g_5$) fit of the $y$ distributions.

*3.2. Evolution equations*

Beyond leading order the structure of the evolution equations is complicated [29] by the fact that now both $P_{q\bar{q}}$ and $P_{q_iq_j}^{ND}$, as well as their polarized counterparts $\Delta P_{q\bar{q}}$ and $\Delta P_{q_iq_j}^{ND}$ no longer vanish: at next-to-leading order they are all given by the diagram displayed in Fig. 1. Furthermore, already at NLO $P_{q\bar{q}}^{ND} \neq P_{qq}^{D}$, because [34] there are two identical quarks in the final state in the diagonal transition, but not in the non-diagonal one. However,

$$P_{q\bar{q}}^{ND,\,\mathrm{NLO}} = P_{qq}^{ND,\,\mathrm{NLO}}, \tag{3.6}$$

because at this order both processes proceed through the diagram of Fig. 1.

Coming to the polarized case, it is useful to recall that unpolarized and polarized splitting functions are respectively [28] the sum and difference of helicity conserving and helicity flipping transitions:

$$P = P^{\uparrow\uparrow} + P^{\uparrow\downarrow}, \quad \Delta P = P^{\uparrow\uparrow} - P^{\uparrow\downarrow}, \tag{3.7}$$

where the arrows here refer to the helicities of the parton before and after the splitting. Due to the collinearity of the splitting, parallel (antiparallel) helicities are equivalent to parallel (antiparallel) spins. Because the quark-gluon coupling conserves helicity, it follows that in the helicity-flipping transition there are two identical particles in the final state (including the spin quantum number), but not in the helicity conserving one. Therefore,

$$P_{q\bar{q}}^{D\,\uparrow\downarrow} \neq P_{q\bar{q}}^{ND\,\uparrow\downarrow}, \tag{3.8}$$

but not for the opposite spin configuration: in fact,

$$P_{q\bar{q}}^{D\uparrow\uparrow,\,\mathrm{NLO}} = P_{q\bar{q}}^{ND\uparrow\uparrow,\,\mathrm{NLO}}; \tag{3.9}$$

$$P_{q\bar{q}}^{ND\uparrow\uparrow,\,\mathrm{NLO}} = P_{q\bar{q}}^{ND\uparrow\downarrow,\,\mathrm{NLO}} = P_{qq}^{ND\uparrow\uparrow,\,\mathrm{NLO}} = P_{qq}^{ND\uparrow\downarrow,\,\mathrm{NLO}}; \tag{3.10}$$

$$P_{qq}^{ND\uparrow\downarrow,\,\mathrm{NLO}} = P_{qq}^{D\uparrow\downarrow,\,\mathrm{NLO}}, \tag{3.11}$$

where the second equation follows from the fact that the equality of splitting functions eq. (3.6) holds for any spin configuration, and the last equation is a consequence of the fact that, because of helicity conservation, the flavor-diagonal but spin-flip splitting also proceeds only through the diagram displayed in Fig. 1.

Now, eq. (3.8) immediately implies that the C–even and C–odd nonsinglet splitting functions are not the same: $\Delta P_{NS}^{+} \neq \Delta P_{NS}^{-}$, like [34] their unpolarized counterparts. However, using eq. (3.10) in the explicit expression for the nonsinglet splitting functions eq. (2.19) it immediately follows that

$$\Delta P_{NS}^{-,\,\mathrm{NLO}} = \Delta P_{S}^{-,\,\mathrm{NLO}} = \Delta P_{qq}^{D,\,\mathrm{NLO}} - \Delta P_{q\bar{q}}^{D,\,\mathrm{NLO}} \equiv \Delta P^{-,\,\mathrm{NLO}} \tag{3.12}$$

and similarly for their unpolarized counterparts (with $\Delta P \to P$). Namely, at next-to-leading order there is only one C–odd polarized (and one unpolarized) splitting function, and thus each C–odd distribution $\Delta q_i^-$ eq. (2.13) for the $i$-th flavor evolves independently:

$$\frac{d}{dt}\Delta q_i^- = \frac{\alpha_s(t)}{2\pi}\Delta P^- \otimes \Delta q_i^-. \tag{3.13}$$

The difference between singlet and nonsinglet C–odd splitting functions starts at order $\alpha_s^2$, but is expected to be very small [35] at that order.

Therefore, at next-to-leading order the full set of evolution equations is given by supplementing the standard singlet and nonsinglet C–even evolution equations eq. (2.16) with the C–odd evolution equation eq. (3.13). The two-loop polarized splitting functions have been computed recently [23], and are specifically discussed in the AB and related factorization schemes in Ref. [33]. The C–odd splitting function, and in fact all the nonsinglet splitting functions [36], can be determined from their unpolarized counterparts. Indeed, using respectively eq. (3.9) and (3.11) in the definitions of eq. (2.7) of $\Delta P_{q\bar{q}}^{NS}$ and $\Delta P_{qq}^{NS}$ we get

$$\begin{aligned} \Delta P_{qq}^{NS,\,\mathrm{NLO}} &= P_{qq}^{NS\uparrow\downarrow,\,\mathrm{NLO}} = P_{qq}^{NS,\,\mathrm{NLO}} \\ \Delta P_{q\bar{q}}^{NS,\,\mathrm{NLO}} &= -P_{q\bar{q}}^{NS\uparrow\downarrow,\,\mathrm{NLO}} = P_{q\bar{q}}^{NS,\,\mathrm{NLO}}, \end{aligned} \tag{3.14}$$

which imply

$$\Delta P_{NS}^{\pm,\,\mathrm{NLO}} = P_{NS}^{\mp,\,\mathrm{NLO}}. \tag{3.15}$$

In Mellin space, the anomalous dimensions

$$\gamma_{NS}(N) \equiv \int_0^1 dx\, x^{N-1} P_{NS}(x) \tag{3.16}$$

do not admit an analytic continuation for all $N$; however, their even and odd moments can be analytically continued separately for all $N$. Because even (odd) moments correspond to C–even (C–odd) operators, the respective analytic continuations give the moments of $P_{NS}^{+} = \Delta P_{NS}^{-}$ and $P_{NS}^{-} = \Delta P_{NS}^{+}$ [34]. Equations (3.9)-(3.11) and their consequences hold in the $\overline{\mathrm{MS}}$ scheme, and remain valid in schemes, such as the AB scheme [33] where the nonsinglet and C–odd quark anomalous dimensions are the same as in $\overline{\mathrm{MS}}$.

## 4. Theoretical expectations and constraints

Even though neutral–current structure function data do not give any information on the relative size of quark and antiquark (or 'valence' and 'sea') distributions, some experimental information is available from semi-inclusive polarized experiments [37]. However, the only conclusion which can be drawn from these experiments at present is that the first moments of the $\Delta\bar{u}(x)$ and $\Delta\bar{d}(x)$ distributions are much smaller than the C–even combinations $\Delta u(x)+\Delta\bar{u}(x)$ and $\Delta d(x)+\Delta\bar{d}(x)$, and in fact compatible with zero. When the same data are folded in a global NLO analysis [38] they lead to an indication that the first moment of the $\Delta\bar{u}(x)$ distribution is positive, and roughly 10% of the first moment of $\Delta u(x)+\Delta\bar{u}(x)$, but since this is smaller than the typical systematic uncertainties on polarized first moments [4] the only solid conclusion that can be drawn from this is, again, that the light antiquark distributions are significantly smaller than the C–even combinations measured in inclusive experiments. Therefore, a wide variety of theoretical scenarios is compatible with present-day data. However, even in the absence of experimental information, some constraints on the relative size of the $\Delta q$ and $\Delta\bar{q}$ distributions are imposed by the requirement of positivity of physical cross–sections.

### *4.1. Positivity bounds*

Positivity bounds [39] on polarized structure functions follow from their definition in terms of a difference of cross–sections eq. (2.6), while their unpolarized counterparts are defined from the sum of the same cross–sections. Expressing structure functions in terms of parton distributions then leads to bounds on the parton distributions themselves. If the leading–order expressions of structure functions are used, these bounds coincide with those which are obtained in the naive parton model by interpreting parton densities as (positive-semidefinite) number densities, while beyond leading order they differ from the naive partonic bounds by a calculable amount. Of course, given accurate measurements of all the relevant quantities, positivity will take care of itself, *i.e.* it will just be a trivial consequence of the fact that cross–sections are positive. However, in the presence of incomplete information, positivity imposes nontrivial bounds on the possible outcomes of future experiments.

In Ref. [39], positivity bounds on the C–even quark distributions and the gluon were derived from their definitions in terms of virtual photon DIS, while it was mentioned (but not proven) that charged–current DIS implies similar bounds on quark and antiquark distributions separately. In order to prove such bounds, it is enough to consider the cross–section asymmetry for gauge boson-hadron scattering $A_1$, analogous to that discussed in Ref. [39], but with the $\gamma^*$ beam replaced by a $W^\pm$ beam. To this purpose, consider the cross–section for scattering of a $W$ with helicity $\lambda_W$ off a hadron with helicity $\lambda_p$, given by

$$\sigma^{W^\pm}(\lambda_W,\lambda_p)=K\epsilon^\mu(\lambda_W)\epsilon^{\nu *}(\lambda_W)W^{W^\pm}_{\mu\nu}(\lambda_p), \tag{4.1}$$

where $K$ contains the coupling constants and the flux and phase-space factors. The polarization vector is $\epsilon^\mu(\pm1)=\frac{1}{\sqrt{2}}(0,1,\pm i,0)$.

A straightforward calculation using the definition eq. (2.1) of the hadronic tensor leads

to

$$\sigma^{W^\pm}(\lambda_W, \lambda_p) = K\left[\left(F_1^{W^\pm} - \lambda_W F_3^{W^\pm}/2\right) + \lambda_p\left(g_5^{W^\pm} + \lambda_W g_1^{W^\pm}\right)\right]. \tag{4.2}$$

Therefore, we get

$$\begin{aligned} A_1^{W^\pm}(\lambda_W, x, Q^2) &\equiv \frac{\sigma(\lambda_W, -1) - \sigma(\lambda_W, +1)}{\sigma(\lambda_W, -1) + \sigma(\lambda_W, +1)} \\ &= -\frac{g_5^{W^\pm}(x, Q^2) + \lambda_W g_1^{W^\pm}(x, Q^2)}{F_1^{W^\pm}(x, Q^2) - \lambda_W F_3^{W^\pm}(x, Q^2)/2}. \end{aligned} \tag{4.3}$$

The asymmetry eq. (4.3) is equal to half (because of the factor discussed after eq. (2.7)) the ratio of the cross-sections eq. (2.6) and (2.4) evaluated at $y = 1$. This is a consequence of the fact that when $y = 1$ the lepton and the gauge boson are collinear, and their helicities must then be aligned by helicity and momentum conservation, so $\lambda_W = \lambda_\ell$.

The leading order positivity bounds now follow immediately by noticing that, because of eq. (2.10) and its unpolarized counterpart, the four combinations in the numerator and denominator correspond respectively to the sum over generations of the two unpolarized and polarized flavors and antiflavors in each generation: *e.g.*, above top threshold

$$|A_1^{W^+,\,\mathrm{LO}}(-1, x, Q^2)| = \frac{\left|\Delta d(x, Q^2) + \Delta s(x, Q^2) + \Delta b(x, Q^2)\right|}{d(x, Q^2) + s(x, Q^2) + b(x, Q^2)} \leq 1. \tag{4.4}$$

The three other combinations give the analogous expressions for $u$–type quarks and for the $u$–type and $d$–type antiquarks. Because the bound $|A_1| \leq 1$ must be satisfied as a matter of principle for any choice of target, below and above each threshold, and also for the process where the flavor of the final–state quark is tagged, we immediatley get the bounds of Ref. [39]

$$|\Delta q_i(x, Q^2)| \leq q_i(x, Q^2); \qquad |\Delta \bar{q}_i(x, Q^2)| \leq \bar{q}_i(x, Q^2) \tag{4.5}$$

for any flavor $i$. It is easy to see that these conditions are sufficient to ensure positivity of the physical lepton–hadron cross–section. Indeed, using the leading–order expression of the structure functions eq. (2.10) in the cross–section eq. (2.4),(2.6), the positivity conditions for the $\nu$–hadron cross section is

$$|\Delta\bar{u} - (y-1)^2 \Delta d| \leq \bar{u} - (y-1)^2 d, \tag{4.6}$$

which is manifestly true if eq. (4.5) holds. Similar conditions hold for the other choices of lepton beam.

As discussed in Ref. [39], the Altarelli-Parisi equations (2.16) imply that if the positivity bounds are respected at some scale $Q_0^2$ by a given set of polarized and unpolarized parton distributions, they will also be respected by the same parton distributions for all $Q^2 > Q_0^2$. Conversely, this implies that the bounds will always be violated at sufficiently low scale. However, at low scale the leading–order approximation breaks down, and it is necessary to consider higher-order corrections. When the next-to-leading order expressions of the structure functions eq. (3.3) are used, the positivity bounds are best written

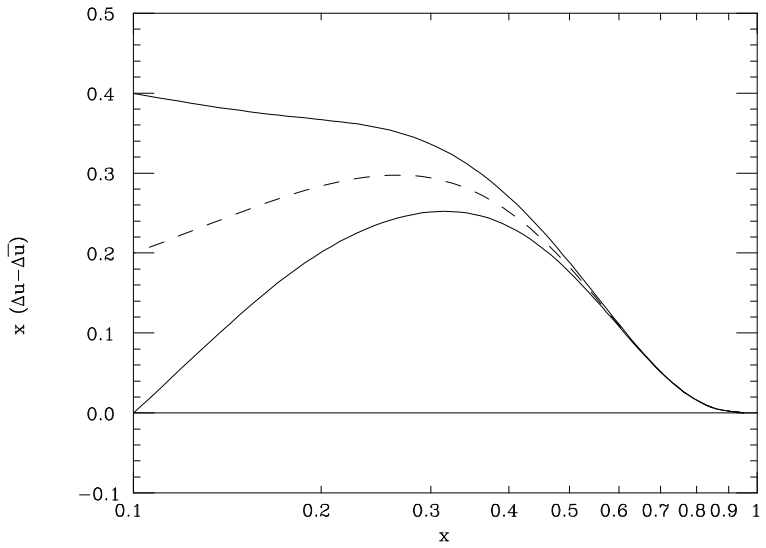


Figure 2: Leading–order positivity bounds for the C–odd up distribution (solid). The $\Delta\bar{u} = 0$ curve (dashed) is also shown.

in terms of the Mellin transforms (defined as in eq. (3.16)) of the coefficient functions and parton distributions, so that all convolutions turn into ordinary products. In such case, the next-to-leading order bound eq. (4.4), including for simplicity only the lightest flavor (as one gets below charm threshold neglecting Cabibbo-suppressed contribution) becomes

$$\frac{\left|\left[1+\frac{\alpha_s}{4\pi}\left(\Delta C_q^{(1)}+\Delta C_5^{(1)}\right)\right]\Delta d+\frac{\alpha_s}{4\pi}\left(\Delta C_q^{(1)}-\Delta C_5^{(1)}\right)\Delta\bar{u}+\frac{\alpha_s}{2\pi}\Delta C_g^{(1)}\Delta g\right|}{\left[1+\frac{\alpha_s}{4\pi}\left(C_q^{(1)}+C_3^{q\,(1)}\right)\right]d+\frac{\alpha_s}{4\pi}\left(C_q^{(1)}-C_3^{(1)}\right)\bar{u}+\frac{\alpha_s}{2\pi}C_g^{(1)}g}\leq 1, \quad (4.7)$$

where $C_q$, $C_g$ and $C_3$ are the unpolarized $F_1$ and $F_3$ coefficient functions, and all parton distributions are functions of $Q^2$ and the Mellin variable $N$.

The impact of the gluon correction on the quark positivity bounds has been extensively discussed in Ref. [39]. Because gluons only mix with the C–even combination of quark distributions, and thus enter eq. (4.7) through the $g_1$ contribution, the conclusions of that reference are unchanged. Namely, because the gluon distribution is peaked at small $x$, the correction to the leading–order positivity bound is only sizable for small moments $N \sim 1.5$, but there the bound itself is very loose because $g(N)$ and $q(N)$ diverge as $N \to 1$ while $\Delta g(N)$ and $\Delta q(N)$ remain finite, so there is no bound as $N \to 1$. Thus, unless the scale is outside the perturbative region (for instance $Q^2 \lesssim 1$ GeV$^2$), gluon-driven next–to–leading order corrections to the positivity bound are essentially negligible. On top of gluon corrections, eq. (4.7) also contains a correction due to the fact that the quark coefficient functions for $g_1$ and $g_5$ are not the same, as per eq. (3.5). This difference, however, is actually quite small and rapidly decreasing at large $x$: indeed, from eq. (3.5) we get that $\Delta C_5^{(1)}(N) - \Delta C_q^{(1)}(N) = \frac{1}{(N+1)(N+2)}$. Hence even at $Q^2 \sim 1$ GeV$^2$ where $\alpha_s \sim 0.5$, and even for, say, $N = 1.5$ the correction is around 1%, and rapidly decreasing as $N$ increases: but, again, at low $N$ the bound is not relevant because of the vanishing of $\frac{\Delta q_i(N)}{q_i(N)}$ as $N \to 1$.

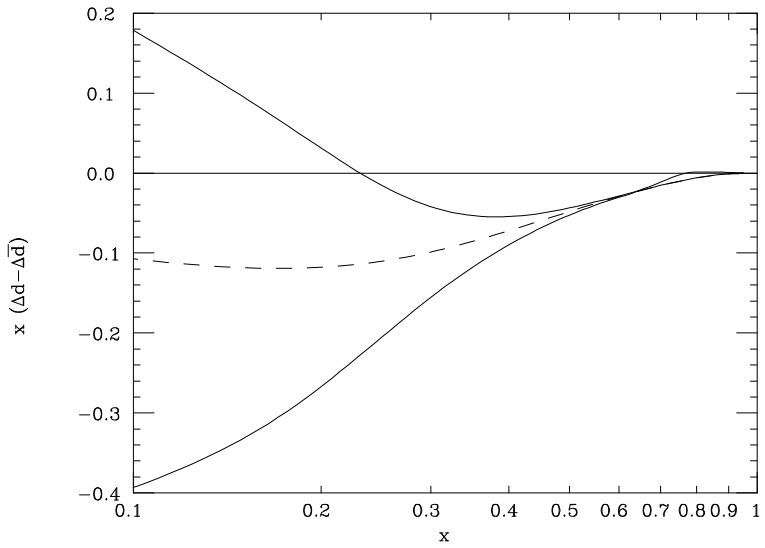


Figure 3: Leading–order positivity bounds for the C–odd down distribution (solid). The $\Delta\bar{d} = 0$ curve (dashed) is also shown.

Hence, to very good approximation, the next-to-leading order positivity bounds are

$$\left|\frac{\Delta q(N)}{q(N)}\right| \leq \frac{1 + \frac{\alpha_s}{2\pi} C_q^{(1)}(N)}{1 + \frac{\alpha_s}{2\pi} \Delta C^{(1)}(N)}, \tag{4.8}$$

*i.e.* the only significant correction to the leading–order bound is due to the fact that the polarized and unpolarized quark coefficient functions are unequal to NLO. Because however $\lim_{N\to\infty} \frac{C_q^{(1)}(N)}{\Delta C^{(1)}(N)} = 1$, this difference is again only significant if $N$ is not too large: in practice, the correction was shown in Ref. [39] to lead to a modification of a few percent of the leading–order bound for moments around $N \sim 5$, where positivity bounds can be relevant. We conclude that for all practical purposes it is enough at the present stage to consider leading–order positivity bounds, since next–to–leading corrections, in the form of eq. (4.8), are only relevant at the level of accuracy of a few percent, and then only for a limited range of moments, relevant for the description of the shape of the parton distributions when $x \gtrsim 0.1$.

Using the experimentally measured values of the unpolarized parton distributions and the polarized C–even distributions, we can then turn the pair of positivity bounds eq. (4.5) on quark and antiquark distributions for each flavor into a bound on the admissible value of the unknown C–odd quark distribution $\Delta q_i^-$ eq. (2.13). The uncertainty on the bound will be dominated by, and thus essentially of the same size as, that on the polarized quark distributions [5], which are much more poorly known than the unpolarized ones. In Figs. 2-4, we show the positivity bounds on the up, down and strange distributions at $Q^2 = 5$ GeV$^2$ obtained in this way by using the CTEQ5 [40] unpolarized up and down quark and antiquark distributions and the BPZ [41] strange distribution, and the polarized parton distributions from Ref. [4]. Use of the BPZ fit is motivated by the fact that in this fit a particularly accurate determination of the unpolarized strange quark and antiquark distributions was achieved by means of a detailed analysis of available neutrino DIS data,

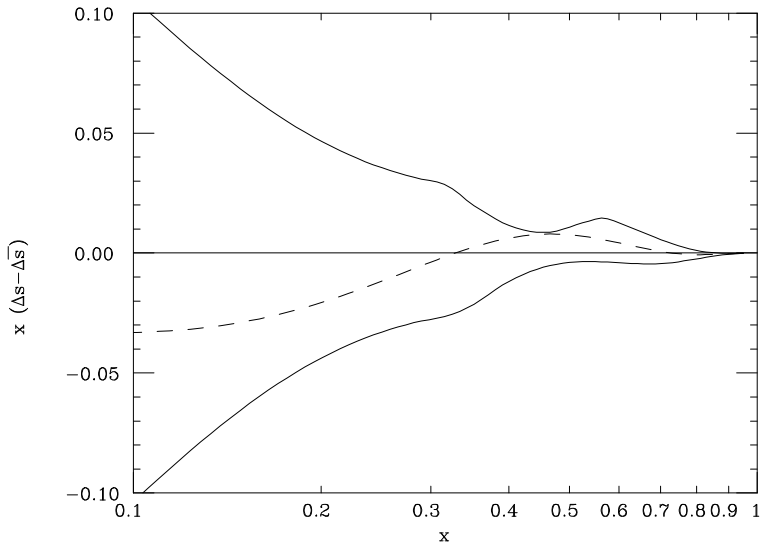


Figure 4: Leading–order positivity bounds for the C–odd strange distribution (solid). The $\Delta\bar{s} = 0$ curve (dashed) is also shown.

whereas a separate determination of the strange quark is not attempted by the CTEQ group (which only determines an SU(3) symmetric sea with corrections for the $\bar{u} - \bar{d}$ asymmetry). In fact, it turns out that the C–even polarized distribution from Ref. [4] is incompatible with the leading–order positivity bound obtained from the CTEQ5 unpolarized strange distribution at large $x$ ($x \gtrsim 0.5$). Even though the violation is within theoretical errors, it is suggestive that no such violation is found when the nominally more accurate BPZ strange distribution is used.

In Figs. 2-4, we also display the $\Delta q_i^- = \Delta q_i^+$, *i.e.* $\Delta\bar{q}_i = 0$ curve for each flavor (dashed curves). It is clear that a large value of the antiquark distribution is not compatible with positivity for both the up and down quark distributions. Indeed, the curve $\Delta\bar{q} = \Delta q$ (*i.e.* $\Delta q^- = 0$) violates the positivity bound for the up quark when $x \gtrsim 0.1$ and for the down quark when $x \gtrsim 0.2$, while when $x \approx 0.3$ only a very small value of the polarized antiquark distribution is allowed (about an order of magnitude smaller than the polarized quark distribution). On the other hand, a vanishing light antiquark distribution is compatible with positivity for all $x$. In the case of the strange distribution, instead, both $\Delta\bar{s} = 0$ and $\Delta\bar{s} = \Delta s$ (or indeed $\Delta\bar{s} = -\Delta s$) are compatible with positivity. As one should expect, for the strange polarized distribution, positivity does not force the antiquark to be smaller than the quark distribution.

### *4.2. Theoretical scenarios and the spin of the proton*

As we have already mentioned in the introduction, one of the main reasons of interest in polarized quark distributions is the unexpected smallness of the nucleon axial charge which has been determined in the first generation of polarized DIS experiments. A clarification of the physics behind this requires a determination of the detailed polarized parton content of the nucleon. A review of the various explanations which have been proposed for this experimental fact is beyond the scope of this work. However, it is useful to sketch various scenarios for the polarized content of the nucleon which are representative of possible

theoretical alternatives, and which could be tested in future experiments.

Firstly, it should be noticed that even though current data give a value of the axial charge which is compatible with zero, they cannot exclude a value as large as $a_0(10\ \mathrm{GeV}^2) = 0.3$ [4]. Also, the current value is obtained by using information from hyperon $\beta$–decays and SU(3) symmetry. Clearly, the theoretical implications of an exact zero are quite different from those of a value which is just smaller than expected in quark models. It is thus important to have a direct determination of the axial charge. If a small value is confirmed, it could be understood as the consequence of a cancellation between a large value of the scale–independent (*i.e.* AB–scheme) quark first moment, and a large gluon first moment. Indeed, since in the $\overline{\mathrm{MS}}$ scheme the axial charge and singlet quark first moment coincide [32], eq. (3.4) is immediately seen to imply that a large gluon contribution can lead to a small value of the axial charge even when the AB–scheme quark is large. In this ('anomaly') scenario the up, down and strange polarized distributions in the AB–scheme are close to their expected quark model values, so in particular the strange distribution is much smaller than the up and down distributions. In Ref. [42], this cancellation of quark and gluon components has been derived from the topological properties of the QCD vacuum [42] (and thus further predicted to be a universal property of all hadrons).

If instead the polarized gluon distribution is small, the smallness of the singlet axial charge can only be explained with a large and negative strange distribution. In this case, the scale–independent first moment of the singlet quark distribution is also small. This scale–independent suppression of the axial charge might be explained by invoking non–perturbative mechanisms based on instanton–like vacuum configuration [43]. In this 'instanton' scenario the strange polarized distribution is large and equal to the anti-strange distribution, since gluon-induced contributions must come in quark–antiquark pairs.

Another scenario is possible, where the smallness of the singlet axial charge is due to intrinsic strangeness, *i.e.* the C-even strange combination is large, but the sizes of $\Delta s$ and $\Delta\bar{s}$ differ significantly from each other. Specifically, it has been suggested that while the strange distribution (and specifically its first moment) is large, the antistrange distribution is much smaller, and does not significantly contribute to the nucleon axial charge [44]. This way of understanding the nucleon spin structure is compatible with Skyrme models of the nucleon, and thus we will refer to this as a 'skyrmion' scenario [6].

Therefore, the main qualitative issues which are relevant for the nucleon spin structure are to assess how small the axial charge is, to determine whether the polarized gluon distribution is large, and then whether the strange polarized distribution is large, and whether the strange polarized quark and antiquark distributions are equal to each other or not. More detailed scenarios might then be considered, once the individual quark and antiquark distributions have all been accurately determined. For instance, while the up and down antiquark distributions are small, they need not be zero, and in fact they could be different from each other [45], just like their unpolarized counterparts appear to be. Investigating these issues could shed further light on the detailed structure of polarized nucleons.

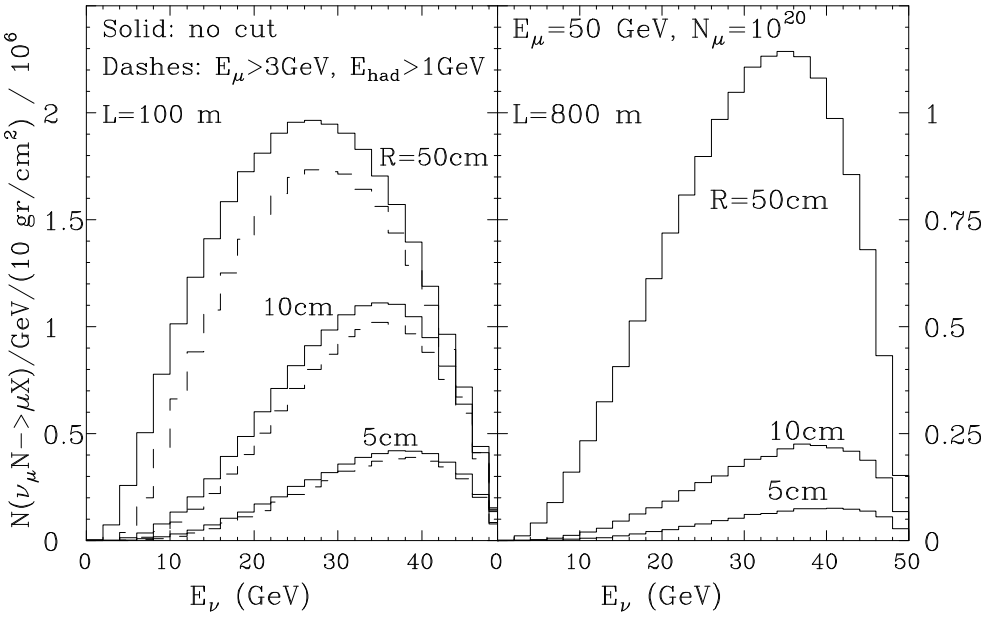


Figure 5: Charged–current event rates, in units of $10^6$, as a function of Lab-frame neutrino spectra, for several detector and beam configurations. The dashed lines on the left include cuts on the final-state muon ($E_\mu > 3$ GeV) and on the final-state hadronic energy ($E_{had} > 1$ GeV). The solid lines have no energy-threshold cuts applied. The three set of curves correspond to different detector radii (50, 10 and 5 cm, from top to bottom).

## 5. Polarized neutrino-DIS at the front-end of a muon ring

The parameters of a realistic neutrino-factory complex are still under active study, and it is expected that the accelerator configuration will evolve and upgrade in both energy and luminosity after the beginning of operations [46]. For the present study we shall assume the following beam parameters, which are considered as typical of the initial operations of a neutrino factory: muon beam energy, $E_\mu = 50$ GeV; length of the straight section, $L = 100$ meters; distance of the detector from the end of the straight section, $d = 30$ meters; number of muon decays per year along the straight section, $N_\mu = 10^{20}$; muon beam angular divergence, $0.1 \times m_\mu/E_\mu$; muon beam transverse size $\sigma_x = \sigma_y = 1.2$ mm. While the concept of "conservative" cannot be applied to any of the projections for the neutrino factory, it is nevertheless reasonable to expect that should one ever be built, its performance would not be inferior to what assumed here. We also assume a cylindrical detector, with azimuthal symmetry around the beam axis, parametrized by its radius $R = 50$ cm and a thickness of 10 gr/cm$^2$. The collected statistics scales linearly with the detector thickness, while the dependence on other parameters such as the radius or the length of the straight section is clearly more complex.

The neutrino spectra are calculated using standard expressions for the muon decays (see *e.g.* Ref. [15]). For simplicity we shall confine ourselves to the case of $\nu_\mu$ and $\bar{\nu}_\mu$ charged current DIS. The laboratory-frame neutrino spectra, convoluted with the charged–current interaction cross-sections, are shown for several detector and beam configurations in Fig. 5 ($E_\mu = 50$ GeV) and in Fig. 6 ($E_\mu = 100$ GeV).

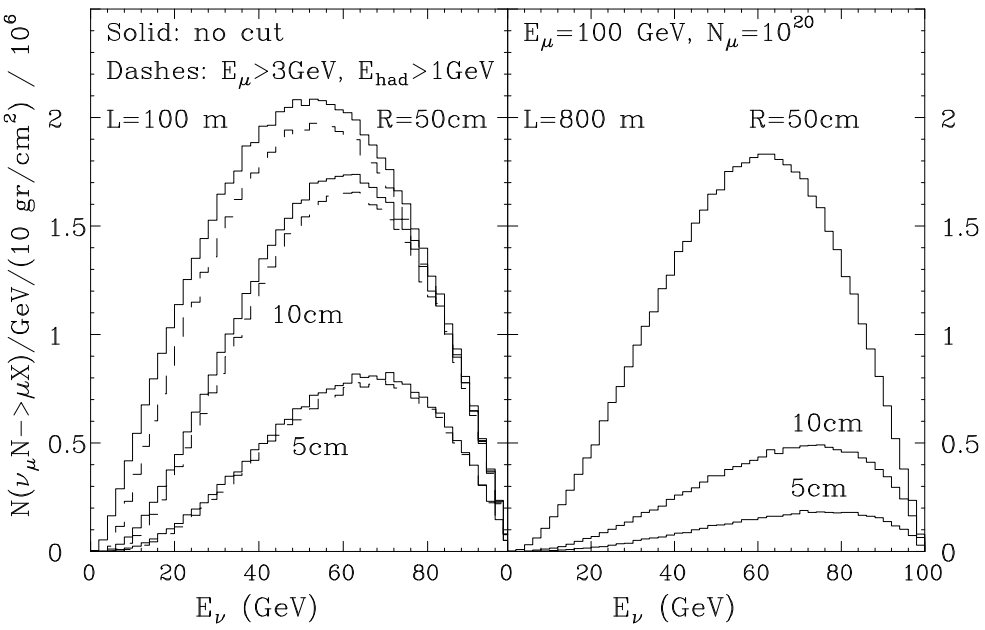


Figure 6: Same as Fig. 5, but for 100 GeV muon beams.

To determine the statistical accuracy with which the individual structure functions and their flavor components are expected to be measured we shall exploit the different $y$ dependence of the separate $F_i$ and $g_i$ components of the cross-section. An important feature of the neutrino beams from muon decays is their wide-band nature. This allows to modulate the $y$ dependence for fixed values of $x$ and $Q^2$ using the neutrino energy:

$$y = \frac{Q^2}{2xmE_\nu}. \tag{5.1}$$

The separate measurement of the recoil muon energy and direction, and of the recoil hadronic energy, enable the event-by-event extraction of $x, y$ and $Q^2$. We assume perfect experimental resolution on the determination of these quantities, after imposing a cut on the minimum energy of the muon ($> 3$ GeV) and of the hadronic system ($> 1$ GeV). Since we are just interested in predicting the statistical accuracy in the determination of the structure functions, we also assume for simplicity the absence of power-suppressed corrections, and impose the Callan-Gross relation. Given the large statistics expected at the neutrino factory, it will nevertheless be possible to use the data to extract the higher-twist components and to separate the individual contributions of $F_1$ and $F_2$ ($g_4$ and $g_5$), without any theoretical assumption. This issue is studied in some detail for the case of unpolarized distributions in Ref. [16].

We thus produced $y$ distributions by generating events within different bins of $x$ and $Q^2$, and performed minimum-$\chi^2$ fits of the generated data using the cross-section eq. (2.4). For each bin, the values of $x$ and $Q^2$ at which we quote the results are obtained from the weighted average of the event rate. As an input, we used the CTEQ4D set of parton distributions [47]. The dependence on the parameterization of the parton distributions is very small, and will be neglected here. We verified that other recent sets of parton

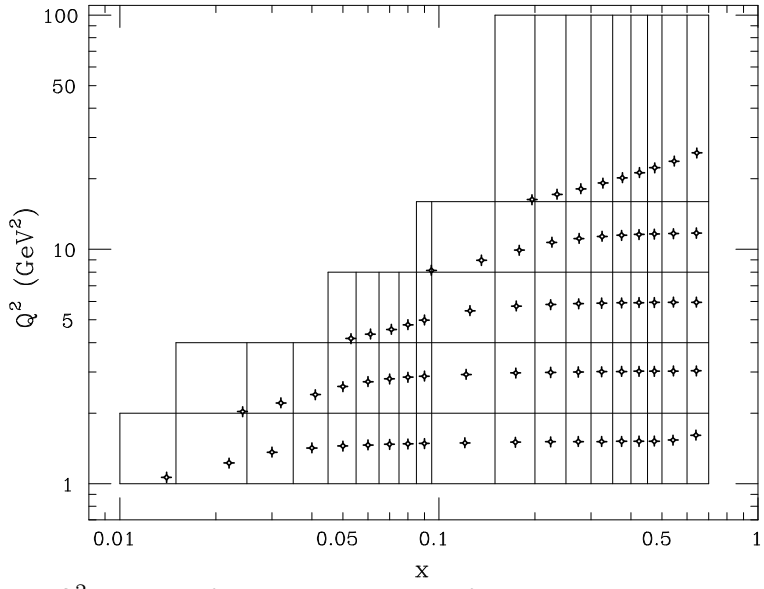


Figure 7: $x$ and $Q^2$ binning for the generation of charged–current events. The crosses correspond to the weighted bin centers.

distributions give similar results. The fit to the $y$ distributions at fixed $x$ and $Q^2$ for a fully polarized target gives then the value of the combinations $F_2 \pm 2xg_5$ and $F_3 \pm 2g_1$.

The absolute number of events expected in each bin is scaled by the total number of muon decays; this number of events determines the statistical error on the individual structure functions obtained through the fit. Polarization asymmetries are extracted by combining data sets obtained using targets with different orientations of the polarization. The statistical accuracies with which the combinations can be performed depend on the statistical content of each individual data set. Since the polarization asymmetries are small relative to the unpolarized cross-sections, the *absolute* statistical uncertainties on the extraction of polarized structure functions will have a very mild dependence on the value of the polarized structure functions themselves; they will be mostly determined by the value of the unpolarized structure functions (which to first approximation fix the overall event rate), and by the polarization properties of the target.

For simplicity, we therefore calculate directly the expected statistical errors $\sigma_{F_2,F_3}$ on the extraction of $F_2$ and $F_3$ using unpolarized targets, and relate them to the errors on the polarized cross sections using the following relation given in [17]:

$$\sigma_{\mathrm{g_i}} = F^{tgt}_{\nu,\bar{\nu}} \sqrt{2}\, \alpha_{ij}\, \frac{\sigma_{\mathrm{F_j}}}{2}, \tag{5.2}$$

where $\alpha_{ij} = 1$ for $(i,j) = (1,3)$ and $\alpha_{ij} = 1/x$ for $(i,j) = (5,2)$, and where $F^{tgt}_{\nu,\bar{\nu}}$ is a correction factor (always larger than one) which accounts for the ratio of the target densities to $H_2$ or $D_2$, for the incomplete target polarization, and for the dilution factor of the target, namely the $\nu$ (or $\bar{\nu}$) cross-section weighted ratio of the polarized nucleon to total nucleon content of the target. The factor of $\sqrt{2}$ in the numerator reflects the need to subtract the measurements with opposite target polarization.

We generate events in the $(x, Q^2)$ bins shown in Fig. 7. Twenty equally-spaced bins in the $0 \leq y \leq 1$ range are used for the $y$ fit. The total number of $x$ bins varies in

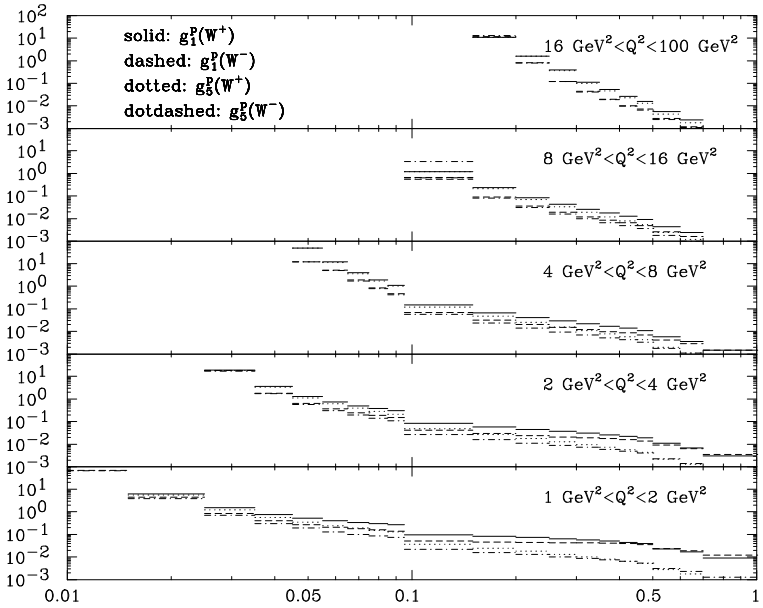


Figure 8: Absolute errors on proton structure functions for the bins of Fig. 7.

different $Q^2$ bins because of kinematic acceptance and minimum energy cuts. The values of the uncertainties in the determination of the eight charged–current structure functions ($g_1$ and $g_5$ with the two available beams and targets) are assigned at the cross-section weighted bin centers. We then get the absolute errors on the structure functions displayed in Figs. 8-9 for proton and deuterium targets respectively, using the p-butanol and D-butanol target [48] correction factors given in Ref. [17], namely $F_\nu^p = 2.6$, $F_{\bar\nu}^p = 1.6$ and $F_{\nu,\bar\nu}^D = 4.4$ (for a more complete discussion of polarized targets and their complementary properties, see [17] and references therein). We have assumed a luminosity of $10^{20}$ muons decaying in the straight section of the muon ring for each charge, for each target, and for each polarization. Assuming that only one polarization and one target can run at the same time, this means eight years of run. While the number of muons may not be dramatically increased, the integration time can be reduced by a large factor if the target thickness can be increased over the conservative 10 gr/cm$^2$ assumed here, or if different targets can be run simultaneously.

## 6. Determination of polarized structure functions at a neutrino factory

We can now study how charged–current DIS data may be used to determine the polarized parton content of the nucleon. The purpose of this exercise is twofold. First, this will give us a first indication of the expected shape and scale–dependence of the charged–current structure functions. Furthermore, on a more quantitative level, we will be able to assess the level of accuracy with which charged–current DIS experiments will allow a determination of individual flavors and antiflavors. Of course, both these tasks can only be achieved by making assumptions on the expected flavor content of the nucleon, and on the expected experimental accuracy. To this purpose, we consider the theoretical scenarios

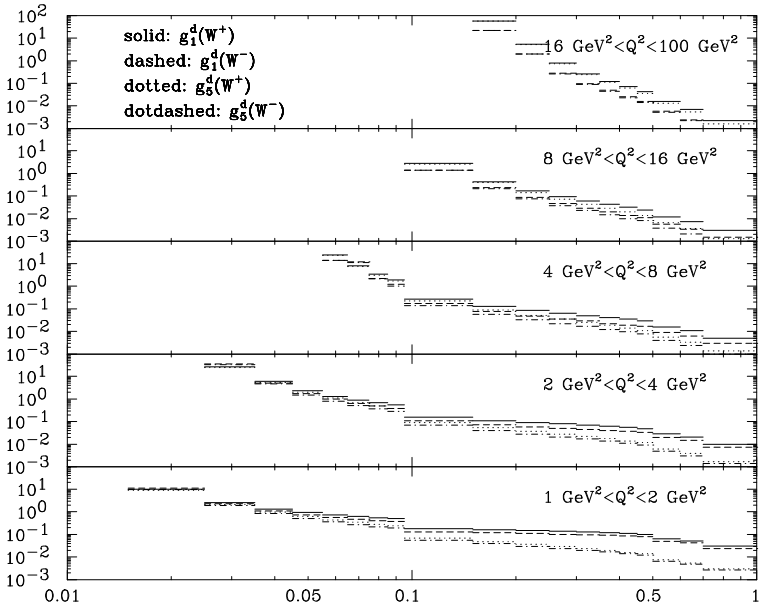


Figure 9: Absolute errors on deuteron structure functions for the bins of Fig. 7.

which we have discussed in Sect. 4, and we assume the availability of data such as discussed in Sect. 5.

In order to implement the theoretical scenarios of Sect. 4, we need to take as a starting point a set of parton distributions which summarize the current knowledge of the polarized structure of the nucleon. To this purpose, we adopt the type–A fit of Ref. [4], which is defined as follows. The C–even polarized quark distributions $\Delta\Sigma^+$ and

$$\begin{aligned} \Delta q_3 &\equiv \Delta q_{ud}^{NS+} \\ \Delta q_8 &\equiv \Delta q_{us}^{NS+} + \Delta q_{ds}^{NS+}, \end{aligned} \tag{6.1}$$

and the polarized gluon distribution $\Delta g$ at the initial scale $Q_0^2 = 1$ GeV$^2$ are all taken to be of the form

$$\Delta f(x, Q_0^2) = \mathcal{N}_f \eta_f x^{\alpha_f} (1-x)^{\beta_f} (1 + \gamma_f x^{\delta_f}), \tag{6.2}$$

where the factor $\mathcal{N}_f$ is such that the parameter $\eta_f$ is the first moment of $\Delta f$ at the initial scale. The nonsinglet quark distributions $\Delta q_3$ and $\Delta q_8$ are assumed to have the same $x$ dependence, while the parameter $\eta_8$, corresponding to the first moment of $\Delta q_8$, is fixed to the value $\eta_8 = 0.579$ from octet baryon decay rates using SU(3) symmetry. Furthermore, $\gamma_\Sigma = \gamma_g = 10$, $\delta_3 = \delta_8 = 0.75$, $\delta_\Sigma = \delta_g = 1$. All other parameters in eq. (6.2) are determined by the fitting procedure.

This set of polarized parton distributions is particularly useful for our present purposes because a detailed analysis of statistical and systematic uncertainties on the first moments based on it was performed in Ref. [4]. The set A is adopted because all parton distributions in this set are amply within positivity bounds [39]. However, some new data [49] from the E155 collaboration, and the final data set from the SMC collaboration have appeared since the publication of Ref. [4]. Therefore, we have repeated the fit including these new data,

in order to ensure that no available information is neglected. This gives us a data set of 176 neutral–current data points.

The best–fit values of the first moments of the C–even parton distributions at the initial low scale $Q_0^2 = 1$ GeV$^2$ thus obtained are listed in the first column of Table 1, together with the errors from the fitting procedure. The fit is performed, and all results are given, in the AB scheme. These values are not far from those of Ref. [4]. They are further affected by theoretical uncertainties, for which we refer to [4]. The detailed shapes of parton distributions are similar to those of Ref. [4], and likewise not very accurately known. As mentioned above, the value of $\eta_8$ in this fit is fixed using the SU(3) flavor symmetry and the measured octet baryon decay constants. Even though the nominal uncertainty on this SU(3) value of $\eta_8$ is relatively small (around 5%), the uncertainty due to failure of exact SU(3) symmetry could be as large as 30% [50]. This effect is taken into account in the estimated theoretical uncertainties given in Ref. [4]. The subsequent three rows of the table give the values of the first moments of $\Delta q(x,Q^2) + \Delta\bar{q}(x,Q^2)$ at $Q^2 = 1$ GeV$^2$ for up, down, and strange, obtained combining the singlet and nonsinglet quark first moments above. Finally, we give in the last row the value of the singlet axial charge $a_0$ at the scale $Q^2 = 10$ GeV$^2$.

Because the first moment of the gluon distribution in this fit is quite large, we can take this global fit as representative of the 'anomaly' scenario discussed in Sect. 4.2, even though the strange distribution is not quite zero. In order to construct parton distributions corresponding to the other scenarios discussed in Sect. 4.2, we have also repeated this fit with the gluon distribution forced to vanish at the initial scale. This possibility is in fact disfavored by several standard deviations; however, once theoretical uncertainties are taken into account a vanishing gluon distribution can only be excluded at about two standard deviations [4], and thus this possibility cannot be ruled out on the basis of present data. The results of this fit for the various first moments are displayed in the second column of Table 1.

We can now use these parton distributions to construct the unknown C–odd parton distributions. We construct three sets of parton distributions, corresponding to the three scenarios of Sect. 4.2. In all cases, we assume $\Delta\bar{u}(x) = \Delta\bar{d}(x) = 0$. Furthermore, as the 'anomaly' set we take the 'generic' fit of Table 1 with the assumption $\Delta\bar{s}(x) = 0$, the strange distribution for this set being relatively small anyway. As 'instanton' and 'skyrmion' parton sets we take the $\Delta g = 0$ fit of Table 1, with $\Delta s = \Delta\bar{s}$ in the former case, and $\Delta\bar{s} = 0$ in the latter case. With these choices all quark and antiquark distributions are fixed, and thus all structure functions can be computed.

We generate for each of these three scenarios a set of pseudo-data, by assuming the availability of neutrino and antineutrino beams, and proton and deuteron targets, in the $(x,Q^2)$ bins of Fig. 7 and with the errors displayed in Figs 8,9. Although experimentally event rates remain sizable even in the large–$x$ region, we do not include data with $x > 0.7$ because, in this region, leading twist next-to-leading order perturbation theory is not reliable. We discard data points whose uncertainty is larger than 50, the typical size of the structure functions being of order one. We finally use these uncertainties to generate data gaussianly distributed about the values of the structure functions at each data point in the three scenarios. We obtain in this way approximately 70 data points for each of the

| par. | generic fit | $\Delta g = 0$ fit | 'anomaly' refit | 'instanton' refit | 'skyrmion' refit |
|---|---|---|---|---|---|
| $\eta_\Sigma$ | $0.38 \pm 0.03$ | $0.31 \pm 0.01$ | $0.39 \pm 0.01$ | $0.321 \pm 0.006$ | $0.324 \pm 0.008$ |
| $\eta_g$ | $0.79 \pm 0.19$ | 0 | $0.86 \pm 0.10$ | $0.20 \pm 0.06$ | $0.24 \pm 0.08$ |
| $\eta_3$ | $1.110 \pm 0.043$ | $1.039 \pm 0.029$ | $1.097 \pm 0.006$ | $1.052 \pm 0.013$ | $1.066 \pm 0.014$ |
| $\eta_8$ | 0.579 | 0.579 | $0.557 \pm 0.011$ | $0.572 \pm 0.013$ | $0.580 \pm 0.012$ |
| $\eta_u$ | 0.777 | 0.719 | $0.764 \pm 0.006$ | $0.722 \pm 0.010$ | $0.728 \pm 0.009$ |
| $\eta_d$ | $-0.333$ | $-0.321$ | $-0.320 \pm 0.008$ | $-0.320 \pm 0.009$ | $-0.325 \pm 0.009$ |
| $\eta_s$ | $-0.067$ | $-0.090$ | $-0.075 \pm 0.008$ | $-0.007 \pm 0.007$ | $-0.106 \pm 0.008$ |
| $a_0$ | $0.183 \pm 0.030$ | $0.284 \pm 0.012$ | $0.183 \pm 0.013$ | $0.255 \pm 0.006$ | $0.250 \pm 0.007$ |

Table 1: Best–fit values of the first moments for the data and pseudodata fits discussed in the text.

eight charged–current structure functions.

We proceed to fit a global set of data which includes the original neutral–current data as well as the generated charged–current data. We assign to the generated data the estimated statistical errors, and fit including statistical errors only. We do not attempt an estimate of the experimental systematic uncertainties, which are very difficult to anticipate: our results are meant to provide a benchmark for the best possible situation of negligible systematics, and set a target of performance for the planned detectors. The errors assigned to the neutral–current data are instead obtained as in our original fits, by adding in quadrature the statistical and systematic errors given by the various experimental groups: a fit including statistical errors only to these data would be very hard to achieve, and somewhat misleading, since the data themselves are affected by the systematics, which cannot be assumed to be absent. Since the statistics is dominated by the generated data, the final errors on the various parameters should be taken as estimates of statistical errors only.

The fits are performed adopting the same functional form and parameters as in the original fit for the C–even parton distributions, except that the normalization of the octet C–even distribution $\eta_8$ is now also fitted. For the C–odd parton distributions, we add six new parameters, namely the normalizations of the up, down and strange C–odd distributions, and three small–$x$ exponents $\alpha$ (corresponding to an $x^\alpha$ small–$x$ behaviour). The shape is otherwise taken to be the same as that of the C–even quark distributions. The exponents $\alpha$ are included among the refit parameters in order for the refitting procedure to be more realistic, in view of the fact that the generated data are distributed around the best fit with appropriate errors, but do not coincide with it. The charm distribution is assumed to vanish below threshold, and to be generated dynamically by perturbative evolution above threshold.

The best–fit values of all the normalization parameters are shown in the last three columns of Table 1, where the rows labelled $\eta_u$, $\eta_d$ and $\eta_s$ now give the best–fit values and errors on the first moments of $\Delta q^-$ for up, down and strange. Comparison of these values with those of our original fits leads to an assessment of the impact of charged–current data on our knowledge of the polarized parton content of the nucleon.

First, we see that the improvement in the determination of the polarized gluon distribution is minor. This is due to the fact that the gluon distribution is determined by scaling violations, and thus a precise determination is only possible using data which cover a wide range of values of $Q^2$. Lacking this, the availability of charged–current data *per se* does not help. Furthermore, since the gluon decouples from $g_5$, the corresponding data do not have any effect on the determination of the gluon distribution. In the 'skyrmion' and 'instanton' fits, where the charged–current data have been generated assuming a vanishing polarized gluon component, the refitted gluon is nevertheless nonzero, though significantly smaller than in the 'anomaly' fit. This is due to the fact that the currently available (neutral–current) data are also included in the refit, and underlines the fact that these data support a gluon distribution which differs significantly from zero. The charged–current data can only have a limited impact in modifying this conclusion for the same reason why they lead to a modest improvement in the precision of the determination of the gluon.

Let us now consider the C–even quark distributions. It is immediately clear that the precision on the singlet quark first moment is very significantly improved by the charged–current data: the error on the first moment of $\Delta\Sigma^+$ is now of a few percent in comparison to about 10% with neutral–current DIS. This follows from the fact that, up to subleading corrections, the singlet quark is directly measured by the combination eq. (2.30) of charged–current structure functions. This improvement is especially significant since the determination of $\eta_\Sigma$ no longer requires knowledge of the SU(3) octet component, unlike that from neutral–current DIS, and it is thus not affected by the corresponding theoretical uncertainty. With this accuracy, the relatively larger value of the singlet quark component found in the 'anomaly' scenario (in the AB scheme) can be experimentally distinguished from the smaller value found in other scenarios, at the level of several standard deviations. In other words, thanks to the charged–current data, it is possible to experimentally refute or confirm the anomaly scenario by testing the size of the scale–independent singlet quark first moment. Correspondingly, the improvement in knowledge of the gluon first moment, although modest, is sufficient to distinguish between the two scenarios.

The determination of the singlet axial charge is improved by an amount comparable to the improvement in the determination of the singlet quark first moment. Its vanishing could thus be established at the level of a few percent. The determination of the isotriplet axial charge is also significantly improved: the improvement is comparable to that on the singlet quark, and due to the availability of the triplet combination of charged–current structure functions eq. (2.28). This would allow an extremely precise test of the Bjorken sum rule, and accordingly a very precise determination of the strong coupling. Finally, the octet C–even component is now also determined with an uncertainty of a few percent. Therefore, the strange C–even component can be determined with an accuracy which is better than 10%. Comparing this direct determination of the octet axial charge to the value obtained from baryon decays would allow a test of different existing models of SU(3) violation [50].

Coming now to the hitherto unknown C–odd quark distributions, we see that the up and down C–odd components can be determined at the level of few percent. This accuracy is just sufficient to establish whether the up and down antiquark distributions, which are constrained by positivity to be quite small, differ from zero, and whether they are equal

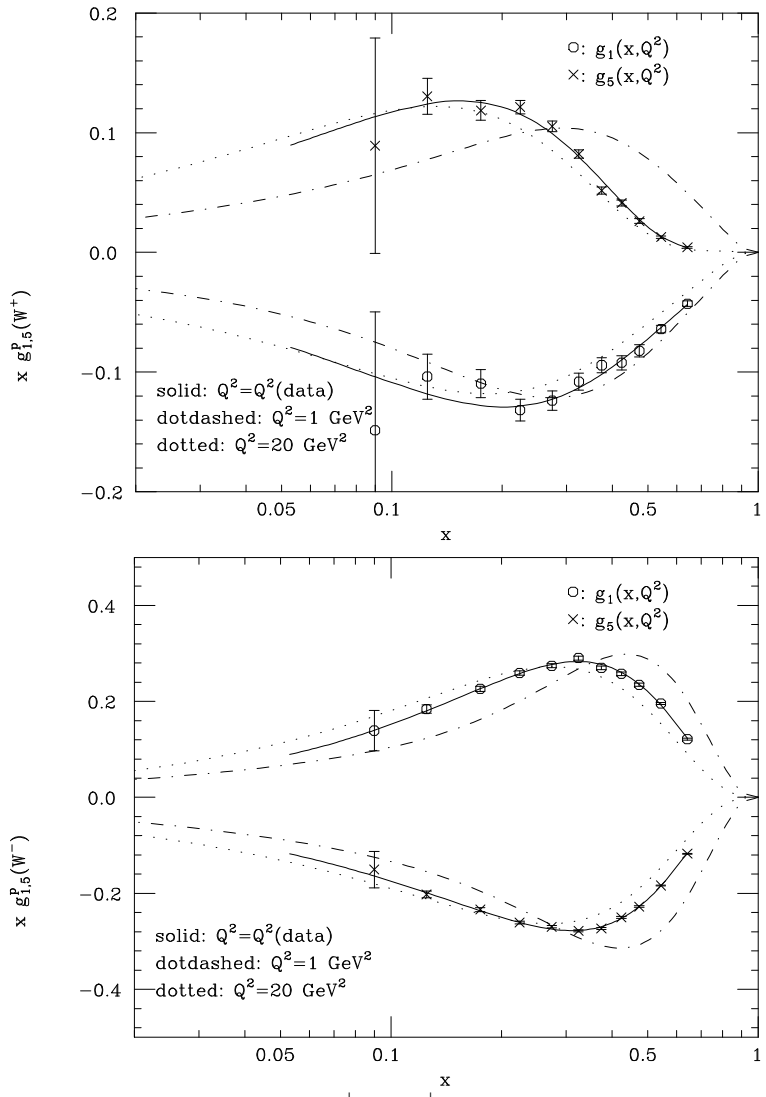


Figure 10: The structure functions $g_1^{W^+}$, $g_5^{W^+}$ (top) and $g_1^{W^-}$, $g_5^{W^-}$ (bottom) for a proton target.

to each other or not. Furthermore, the strange C–odd component can be determined at a level of about 10%, sufficient to test for intrinsic strangeness, *i.e.* whether the C–odd component is closer in size to zero or to the C–even component. The 'instanton' and 'skyrmion' scenarios can thus also be distinguished at the level of several standard deviations.

Of course, only experimental errors have been considered so far. In Ref. [4] it has been shown that theoretical uncertainties on first moments are dominated by the small–$x$ extrapolation and higher–order corrections. The error due to the small–$x$ extrapolation is a consequence of the limited kinematic coverage at small $x$. This will only be reduced once beam energies higher than envisaged in this paper will be achieved; otherwise, this uncertainty could become the dominant one and hamper an accurate determination of first moments. On the other hand, the error due to higher order corrections could be reduced, since it is essentially related to the fact that available neutral–current data must

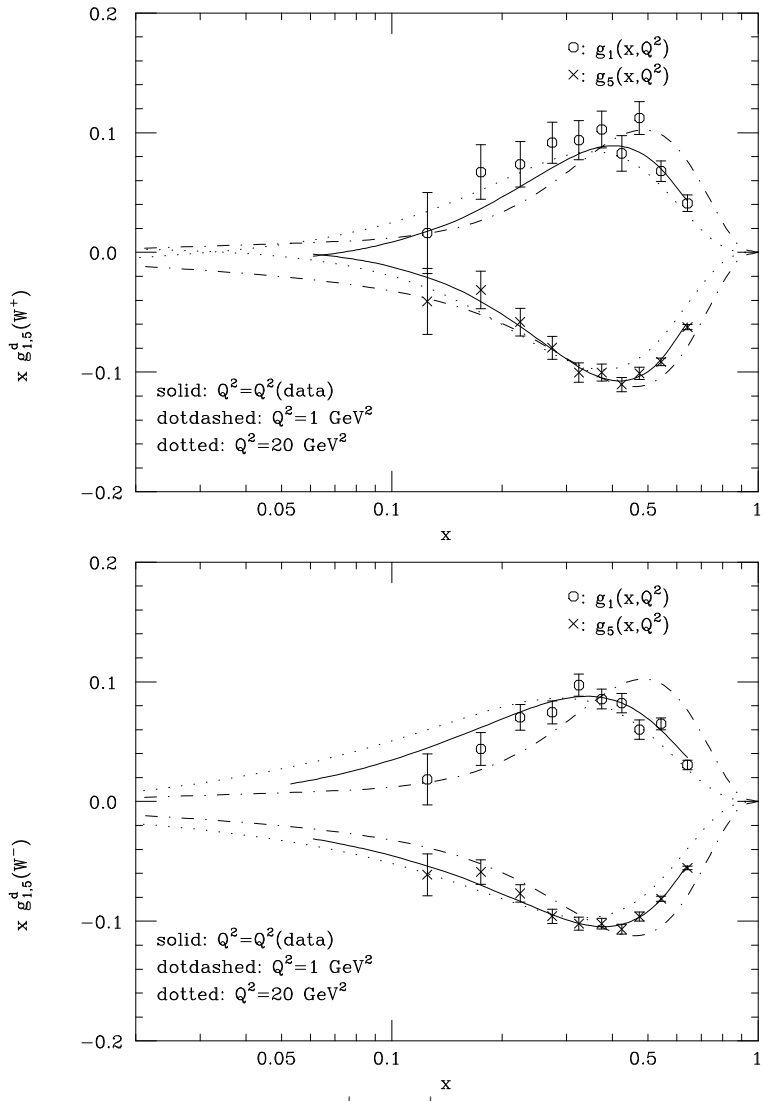


Figure 11: The structure functions $g_1^{W^+}$, $g_5^{W^+}$ (top) and $g_1^{W^-}$, $g_5^{W^-}$ (bottom) for a deuterium target.

be evolved to a common scale, and also errors are amplified [1] when extracting the singlet component from neutral–current data because of the need to take linear combinations of structure functions. Neither of these procedures is necessary if charged–current data with the kinematic coverage considered here are available.

The best–fit structure functions corresponding to the 'anomaly' refit (third column of Table 1) are displayed as functions of $x$ at the scale corresponding to the bin 4 GeV$^2$ $\leq$ $Q^2$ $\leq$ 8 GeV$^2$, and compared with the data in Figs. 10-11 (a few data points with large error bars, although included in the fits, are not shown in the figures). Notice that the structure functions $g_1$ and $g_5$ always have opposite signs because the (dominant) quark component in $g_1$ and $g_5$ has the opposite sign, while the antiquark component has the same sign. For comparison, we also display the structure functions at the initial scale of the fits, and at a high scale. The good quality of the fits is apparent from these plots.

Given the poor quality of current knowledge of the shape of polarized parton distri-

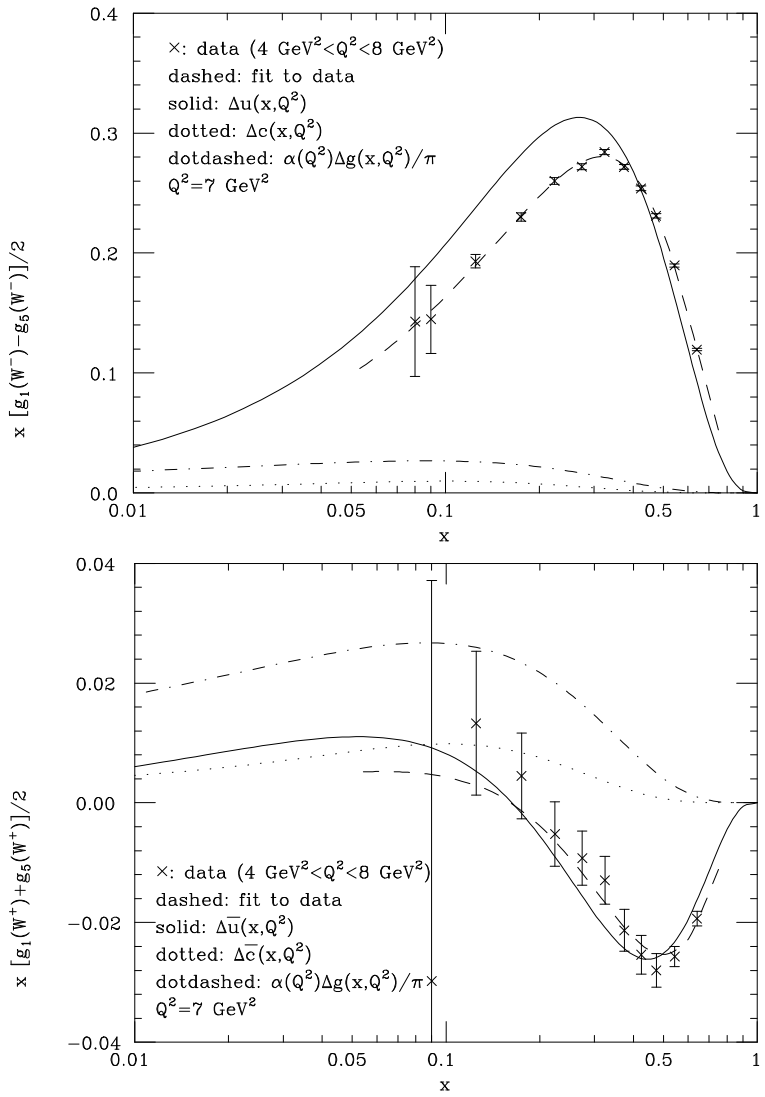


Figure 12: The combinations of structure functions of eq. (2.23), and the corresponding parton distributions.

butions, it is difficult to envisage detailed scenarios and perform a quantitative analysis of the various shape parameter, as we did for first moments. However, it is possible to get a rough estimate of the impact of charged–current data on our knowledge of the $x$ dependence of individual parton distributions by considering the combinations of structure functions given in eqs. (2.23),(2.24), which, at leading order, are directly related to individual parton distributions. In Figs. 12,13 we show, respectively, the combinations of eq. (2.23) and (2.24) for a proton target, together with the pseudodata for the same combinations of structure functions, in the bin $4\ \mathrm{GeV}^2 \leq Q^2 \leq 8\ \mathrm{GeV}^2$. In each figure we also display the two parton distributions which contribute at leading order to the relevant combination of structure functions at $Q^2 = 7\ \mathrm{GeV}^2$, as well as $(\alpha_s/\pi)\Delta g$ at the same scale.

Let us consider the upper plot in Fig. 12. It is apparent that the expected statistical accuracy is very good for all data with $x > 0.1$. This suggests that an accurate determination of the shape of $\Delta u + \Delta c$ is possible. Furthermore, it is also clear that $\Delta c$ (dotted curve)

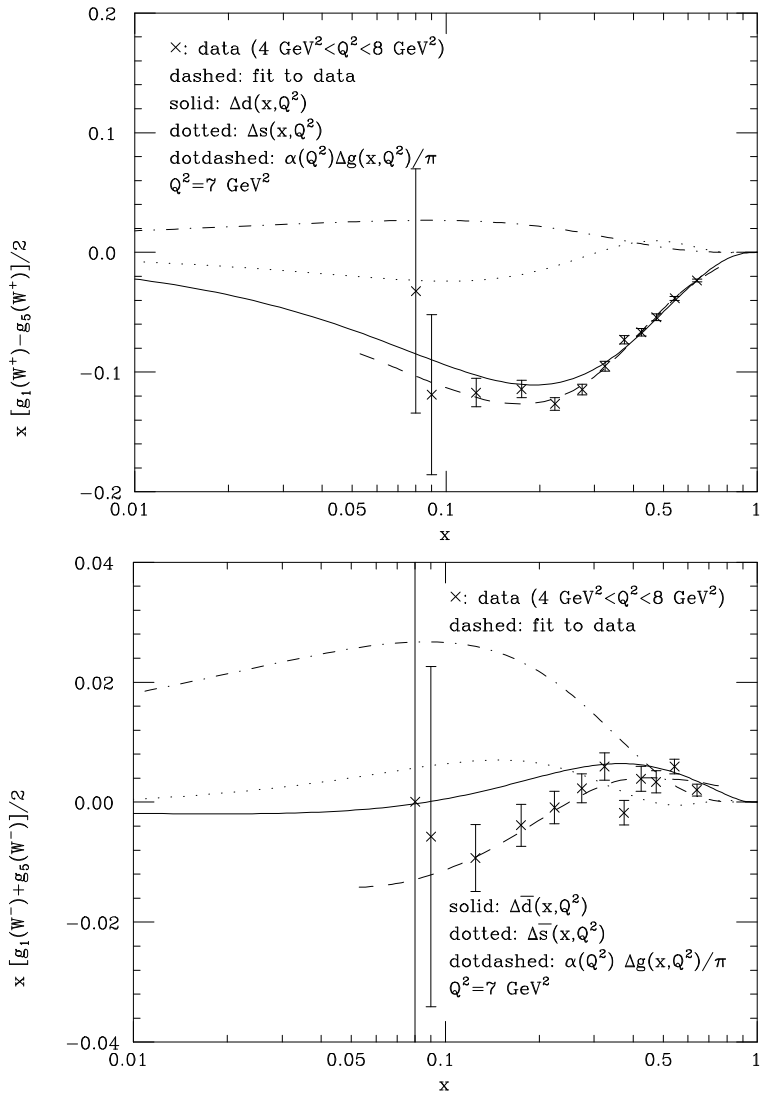


Figure 13: The combinations of structure functions of eq. (2.24), and the corresponding parton distributions.

is extremely small compared to $\Delta u$ (solid curve). However, we observe that the difference between the $\Delta u$ distribution (solid) and the data is of the order of 15% to 20% for all $x$ below 0.4. This difference is entirely due to next-to-leading corrections. Specifically, the gluon contribution (dot-dashed curve), which in the AB scheme spoils the leading order identification of the quark parton distribution with the structure function [see eq. (3.4)], is small but non negligible. Because the various contributions to next-to-leading corrections (in particular the gluon distribution) are affected by sizable theoretical uncertainties [4], this implies that $\Delta u$ can only be determined with an error which is considerably larger than the experimental one. At larger scales, one expects the subleading corrections to coefficient functions to be smaller and smaller, while a residual gluon contribution persists, because of the axial anomaly [32].

A similar analysis of the lower plot of Fig. 12 tells us that a determination of the shape of $\Delta\bar{u}$ is essentially impossible. This combination of structure functions is the preferred

one for a determination of the charm distribution, since perturbatively we expect $\Delta c = \Delta \bar{c}$, and $\Delta \bar{u}$ is much smaller than $\Delta u$. Nevertheless, it is apparent from this figure that even in this case a determination of the charm distribution is out of reach.

A study of the down quark and antiquark distributions can be similarly performed looking at Fig. 13. The conclusion for $\Delta d$ is similar, although perhaps slightly less optimistic, to that for $\Delta u$: a reasonable determination of its shape is possible, but with sizable theoretical uncertainties. The lower plot shows that no significant information on the shape of $\Delta \bar{d}$ can be obtained from this analysis.

## 7. Conclusions and Outlook

We presented in this paper a self-contained review of the next-to-leading order formalism for the description of charged–current polarized DIS, discussing in particular the impact of next-to-leading order corrections to the evolution equations and to the relations between polarized structure functions and polarized parton densities. We discussed the theoretical constraints on individual quark and antiquark polarized distributions emerging from positivity requirements of physical cross-sections. We found that $\Delta \bar{u}(x)$ and $\Delta \bar{d}(x)$ are constrained to be much smaller than the valence polarizations $\Delta u(x)$ and $\Delta d(x)$, respectively; $\Delta \bar{s}(x)$ and $\Delta s(x)$ are instead allowed to have similar size.

We then focused the phenomenological applications to the case of neutrino scattering, which has recently become an intriguing possibility in the context of the neutrino factory facilities being explored world-wide. After evaluating the statistical uncertainties which are expected to be achievable in the measurement of polarized structure functions, we studied the impact of such accuracies on the theoretical models describing the structure of the proton spin. In the case of the C–even distributions, our results indicate that the singlet, triplet and octet axial charges can be measured with accuracies which are up to one order of magnitude better than the current uncertainties. In particular, the improvement in the determination of the singlet axial charge would allow a definitive confirmation or refutation of the anomaly scenario compared to the 'instanton' or 'skyrmion' scenarios, at least if the theoretical uncertainty originating from the small–$x$ extrapolation can be kept under control. The measurement of the octet axial charge with a few percent uncertainty will allow a determination of the strange contribution to the proton spin better than 10%, and allow stringent tests of models of SU(3) violation when compared to the direct determination from hyperon decays.

In the case of C–odd distributions, the up and down components can be determined at the level of few percent, allowing the measurement of an antiup and antidown polarization at levels small enough to be still compatible with the positivity constraints. The strange C–odd component can be measured at the level of 10%, sufficient to test for instrinsic strangeness, and thus distinguish between 'skyrmion' and 'instanton' scenarios at a level of several standard deviations.

We also studied the prospects for the determination of the shape of the polarized distributions. If one were to assume the leading–order relation between structure functions and polarized parton densities, the statistical power of the neutrino factory data would pin down the shape of $\Delta u(x)$ with a few-percent precision. Most of this accuracy is however

lost when next-to-leading order corrections are taken into account, which mix the quark and gluon distributions. The impact of the gluon distribution on the extraction of the $\Delta u(x)$ shape is at the level of 15-20%, and any uncertainty on $\Delta g(x)$ will be reflected on this extraction accordingly. The results for $\Delta d(x)$ are similar to those for $\Delta u(x)$, while no significant shape information can be obtained for the sea distributions. In the case of $\Delta s(x)$ one may be able to use semi-inclusive measurements, with tagged charm quarks in the final state, but this study remains to to be done.

Our analysis did not try to incorporate any estimate of the systematic experimental uncertainties, nor of the theoretical systematics induced by the separation of higher-order and higher-twist contributions, and small-$x$ extrapolation. Likewise, we did not try to include the new information on the spin structure of the proton and on polarized parton densities which might become available through future experiments at CERN, DESY and RHIC. Our study confirms nevertheless the expectation that polarized DIS experiments at a neutrino factory will provide invaluable information on the structure of the proton, provided the experimental systematics will be able to match the statistical one. At the same time, our work stresses the known fact that QCD corrections to the parton-level picture are large, and that a neutrino factory alone may not be able to fully disentangle the shape of individual quark flavors unless a firmer knowledge of the polarized gluon is achieved.

**Acknowledgements**: We thank M. Anselmino, R. D. Ball, P. Gambino, D. Harris, J. Lichtenstadt, K. McFarland and F. Zomer for discussions, and A. Blondel for providing us with the code describing the neutrino beam. This work was supported in part by EU TMR contract FMRX-CT98-0194 (DG 12 - MIHT).

## References


[1] See *e.g.* G. Ridolfi, *Nucl. Phys.* **A666** (2000) 278;
R. D. Ball and H. A. M. Tallini, `hep-ph/9812383`;
S. Forte, `hep-ph/9409416`, `hep-ph/9610238`.

[2] See *e.g.* E. W. Hughes and R. Voss, *Ann. Rev. Nucl. Part. Sci.* **49** (1999) 303;
R. Windmolders, `hep-ph/9905505`.

[3] EMC Collaboration, J. Ashman *et al.*, *Phys. Lett.* **B206** (1988) 364; *Nucl. Phys.* **B328** (1989) 1.

[4] G. Altarelli, R.D. Ball, S. Forte and G. Ridolfi, *Nucl. Phys.* **B496** (1997) 337;
G. Altarelli, R. D. Ball, S. Forte and G. Ridolfi, *Acta Phys. Pol.* **B29** (1998) 1145.

[5] SMC Collaboration, B. Adeva *et al.*, *Phys. Rev.* **D58** (1998) 112002.

[6] S. J. Brodsky, J. Ellis and M. Karliner, *Phys. Lett.* **B206** (1988) 309;
J. Ellis and M. Karliner, `hep-ph/9601280`.

[7] S. Forte, *Acta Phys. Pol.* **B22** (1991) 1065 ;
A. H. Mueller, *Phys. Lett.* **B234** (1990) 517.

[8] J. M. Conrad, M. H. Shaevitz and T. Bolton, *Rev. Mod. Phys.* **70** (1998) 1341.

[9] See *e.g.* T. Benisch, H1 and ZEUS, *Nucl. Phys.* **A666** (2000) 141.

[10] M. Anselmino, P. Gambino and J. Kalinowski, *Phys. Rev.* **D55** (1997) 5841.

[11] The Muon Collider Coll., $\mu^+\mu^-$ *Collider: a feasibility study*, BNL-52503, Fermilab-Conf-96/092, LBNL-38946;
B. Autin, A. Blondel and J. Ellis eds., *Prospective Study of Muon Storage Rings at CERN*, CERN 99-02, ECFA 99-197.

[12] D. M. Kaplan, `physics/0001037`;
B. J. King, `hep-ex/9911008`, `hep-ex/0001043`

[13] S. Geer, *Phys. Rev.* **D57** (1998) 6989, Erratum *ibid.*, **D59** (1999) 039903.

[14] C. Albright *et al.*, *Physics at a neutrino factory*, `hep-ex/0008064.`

[15] I. Bigi *et al.*, *The potential for neutrino physics at muon colliders and dedicated high current muon storage rings*, BNL-67404.

[16] M. L. Mangano *et al.*, QCD/DIS Working Group, to appear in the Report of the CERN/ECFA Neutrino Factory Study Group.

[17] R. D. Ball, D. A. Harris and K. S. McFarland, `hep-ph/0009223`.

[18] M. Anselmino, P. Gambino and J. Kalinowski, *Zeit. Phys.* **C64** (1994) 267.

[19] M. Maul *et al.*, *Zeit. Phys.* **A356** (1997) 443.

[20] J. Blümlein and N. Kochelev, *Nucl. Phys.* **B498** (1997) 285.

[21] D. de Florian and R. Sassot, *Phys. Rev.* **D51** (1995) 6052.

[22] S. Kretzer and M. Stratmann, *Eur. Phys. Jour.* **C10** (1999) 107.

[23] R. Mertig and W. L. van Neerven, *Zeit. Phys.* **C70** (1996) 637;
W. Vogelsang, *Phys. Rev.* **D54** (1996) 2023, *Nucl. Phys.* **B475** (1996) 47.
[24] R. K. Ellis, W. J. Stirling and B. R. Webber, *QCD and Collider Physics* (Cambridge U.P., Cambridge 1996).
[25] D. A. Dicus, *Phys. Rev.* **D5** (1972) 1367;
E. Derman, *Phys. Rev.* **D7** (1973) 2755.
[26] C. G. Callan and D. J. Gross, *Phys. Rev. Lett.* **22** (1969) 156.
[27] S. J. Brodsky *et al.*, *Phys. Lett.* **B93** (1980) 451.
[28] G. Altarelli and G. Parisi, *Nucl. Phys.* **B126** (1977) 298.
[29] See *e.g.* G. Altarelli, *Phys. Rep.* **81** (1982) 1.
[30] E. B. Zijlstra and W. L. van Neerven, *Nucl. Phys.* **B417** (1994) 61
[31] J. Kodaira *et al.*, *Phys. Rev.* **D20** (1979) 627; *Nucl. Phys.* **B159** (1979) 99;
J. Kodaira, *Nucl. Phys.* **B165** (1979) 129.
[32] G. Altarelli and G. G. Ross, *Phys. Lett.* **B212** (1988) 391;
R. D. Carlitz, J. C. Collins and A. H. Mueller,*Phys. Lett.* **B214** (1988) 229;
G. Altarelli and B. Lampe, *Zeit. Phys.* **C47** (1990) 315;
W. Vogelsang, *Zeit. Phys.* **C50** (1991) 275.
[33] R.D. Ball, S. Forte and G. Ridolfi, *Phys. Lett.* **B378** (1996) 255.
[34] D. A. Ross and C. T. Sachrajda, *Nucl. Phys.* **B179** (1979) 497.
[35] W. L. van Neerven and A. Vogt, *Nucl. Phys.* **B568** (2000) 263.
[36] M. Stratmann, A. Weber and W. Vogelsang, *Phys. Rev.* **D53** (1996) 238.
[37] SMC Coll., B. Adeva *et al.*, *Phys. Lett.* **B420** (1998) 180;
HERMES Coll, K. Ackerstaff *et al.*, *Phys. Lett.* **B464** (1999) 123.
[38] D. de Florian and R. Sassot, *Phys. Rev.* **D62** (2000) 094025.
[39] G. Altarelli, S. Forte and G. Ridolfi, *Nucl. Phys.* **B534** (1998) 277; *Nucl. Phys. B (Proc. Suppl.)* **74** (1999) 138.
[40] CTEQ Coll., H. L. Lai *et al.*, *Eur. Phys. Jour.* **C12** (2000) 375.
[41] V. Barone, C. Pascaud and F. Zomer, *Eur. Phys. Jour.* **C12** (2000) 243.
[42] G. M. Shore and G. Veneziano, *Phys. Lett.* **B244** (1990) 75; *Nucl. Phys.* **B381** (1992) 23; see also G. M. Shore, `hep-ph/9812355`.
[43] S. Forte, *Phys. Lett.* **B224** (1989) 189; *Nucl. Phys.* **B331** (1990) 1;
S. Forte and E. V. Shuryak, *Nucl. Phys.* **B357** (1991) 153.
[44] S. J. Brodsky and B.-Q. Ma, *Phys. Lett.* **B381** (1996) 317.
[45] M. Glück *et al.*, `hep-ph/0011215`.
[46] See for example the studies presented at the NuFACT'00 Workshop, May 22-26, Monterey, CA, `http://www.lbl.gov/Conferences/nufact00/`.
[47] CTEQ Coll., H. L. Lai *et al.*, *Phys. Rev.* **D55** (1997) 1280 .
[48] SMC Coll., D. Adams *et al.*, *Nucl. Instrum. Meth.* **A437** (1999) 23.

[49] SMC Coll., B. Adeva *et al.*, *Phys. Rev.* **D58** (1998) 112001 ;
E155 Coll. P. L. Anthony *et al.*, *Phys. Lett.* **B493** (2000) 19.

[50] B. Ehrnsperger and A. Schäfer, *Phys. Lett.* **B348** (1995) 619;
J. Lichtenstadt and H. J. Lipkin, *Phys. Lett.* **B353** (1995) 119;
J. Dai *et al.*, *Phys. Rev.* **D53** (1996) 273;
P. G. Ratcliffe, *Phys. Lett.* **B365** (1996) 383.